Modeling the impact of moulin shape on subglacial hydrology

Celia Trunz[1], Matthew David Covington[2], Kristin Poinar[3], Lauren C Andrews[4], Jessica Mejia[5], and Jason Gulley[6]

[1]Université de Sherbrooke
[2]University of Arkansas at Fayetteville
[3]University at Buffalo, State University of New York
[4]NASA Goddard Space Flight Center
[5]University at Buffalo
[6]University of South Florida

November 22, 2022

Abstract

Subglacial models represent moulins as cylinders or cones, but field observations suggest the upper part of moulins in the Greenland Ice Sheet have more complex shapes. These more complex shapes should cause englacial water storage within moulins to vary as a function of depth, a relationship not currently accounted for in models. Here, we use a coupled englacial–subglacial conduit model to explore how moulin shape affects depth-dependent moulin water storage and water pressure dynamics within a subglacial channel. We simulate seven different moulin shapes across a range of moulin sizes. We find that the englacial storage capacity at the water level is the main control over the daily water level oscillation range and that depth-varying changes in englacial water storage control the temporal shape of this oscillation. Further, the cross-sectional area of the moulin within the daily oscillation range, but not above or below this range, controls pressures within the connected subglacial channel. Specifically, large cross-sectional areas can dampen daily to weekly oscillations that occur in the surface meltwater supply. Our findings suggest that further knowledge of the shape of moulins around the equilibrium water level would improve englacial storage parameterization in subglacial hydrological models and aid predictions of hydro-dynamic coupling.

Modeling the impact of moulin shape on subglacial hydrology

Celia TRUNZ[1], Matthew D. COVINGTON[1], Kristin POINAR[2], Lauren C. ANDREWS[3], Jessica MEJIA[2,4], Jason GULLEY[4]

[1]Geosciences Department, University of Arkansas, Fayetteville AR, USA
[2]Department of Geology, University at Buffalo, Buffalo NY, USA
[3]Global Modeling and Assimilation Office, NASA Goddard Space Flight Center, Greenbelt MD, USA
[4]Geosciences Department, University of South Florida, Tampa FL, USA

Key Points:

- We use a single-conduit subglacial hydrological model to study how moulin size and shape affect subglacial water pressure.
- Subglacial water pressure dynamics are controlled by the moulin cross-sectional area only within the range of daily water level oscillations.
- The englacial void ratio in glacier hydrology models can be represented by the moulin volume within the daily water level oscillation range.

Corresponding author: Celia Trunz, celia.trunz@gmail.com

Abstract

Subglacial models represent moulins as cylinders or cones, but field observations suggest the upper part of moulins in the Greenland Ice Sheet have more complex shapes. These more complex shapes should cause englacial water storage within moulins to vary as a function of depth, a relationship not currently accounted for in models. Here, we use a coupled englacial–subglacial conduit model to explore how moulin shape affects depth-dependent moulin water storage and water pressure dynamics within a subglacial channel. We simulate seven different moulin shapes across a range of moulin sizes. We find that the englacial storage capacity at the water level is the main control over the daily water level oscillation range and that depth-varying changes in englacial water storage control the temporal shape of this oscillation. Further, the cross-sectional area of the moulin within the daily oscillation range, but not above or below this range, controls pressures within the connected subglacial channel. Specifically, large cross-sectional areas can dampen daily to weekly oscillations that occur in the surface meltwater supply. Our findings suggest that further knowledge of the shape of moulins around the equilibrium water level would improve englacial storage parameterization in subglacial hydrological models and aid predictions of hydro-dynamic coupling.

Plain Language Summary

The speed of glacier ice flowing towards the ocean is influenced by timing and the amount of water flowing in moulins. Moulins are large vertical shafts that penetrate the entire ice thickness to transport water from the glacier's surface to the bed. Water levels within moulins reflect the water pressure within channels that form underneath the glacier, transporting meltwater seaward. Most models that are used to simulate this water flow under the ice assume that moulins are cylindrical, but in reality they are not. In this study, we show that non-cylindrical moulins affect how the water level fluctuates within moulins, and that what matters is the shape of the moulin within the range where the water level oscillates.

1 Introduction

In land-terminating regions of the Greenland Ice Sheet, the response of the subglacial drainage system to meltwater inputs is a primary influence on ice motion (e.g., Andrews et al., 2014; Hoffman et al., 2016; Schoof, 2010). Spatial (Banwell et al., 2016) and temporal (Schoof, 2010) variability in supraglacial meltwater input affects subglacial channel water pressures and ice motion. While pressures within subglacial channels tend to control mid-melt-season ice motion, changes in the inefficient subglacial drainage system can influence late-season slowdowns (Andrews et al., 2014; Hoffman et al., 2016; Mejia et al., 2021).

Englacial storage exerts an important control on the pressure dynamics within the subglacial drainage system (Flowers & Clarke, 2002). Storage must be included within some subglacial models to produce realistic oscillation dynamics in channelized subglacial drainage systems (Werder et al., 2013). Storage can affect both the distance over which pressure variations will diffuse away from channels (Werder et al., 2013) and the rate of water pressure rise after the melt season (Downs et al., 2018). Consequently, storage plays a central role in the link between meltwater and ice motion.

Moulins collect nearly all of the supraglacial meltwater on the Greenland Ice Sheet (Smith et al., 2015) and route this meltwater to the most efficient parts of the subglacial drainage system (Gulley et al., 2012). By connecting to subglacial channels, subglacial water pressures are modulated by the water stored within moulins (Banwell et al., 2016; Werder et al., 2013). Moulins represent a potentially large percentage of the englacial

void space that is directly coupled to the subglacial system (Covington et al., 2020). Most subglacial hydrological models treat englacial storage as a spatially uniform and temporally constant model parameter, such as englacial void fraction (Bartholomaus et al., 2011; Hewitt, 2013; Hoffman et al., 2016; Koziol & Arnold, 2018; Stevens et al., 2018; Sommers et al., 2018; Werder et al., 2013). However, limited exploration within moulins in alpine type glaciers (e.g. Gulley et al., 2009; Holmlund, 1988; Vallot, 1898; Vatne & Irvine-Fynn, 2016) and in Greenland (Bourseiller et al., 2002; Covington et al., 2020; Griselin, 1995; Lamberton, 2002; Moreau, 2009) suggests that moulins often have irregular shapes, where storage capacity varies substantially with depth.

In this study, we explore how moulin shape affects water level dynamics in moulins and subglacial channels in a Greenland-type ice sheet using the single-conduit model developed by Covington et al. (2020). Since relatively little is known about specific moulin shapes in Greenland, we explore a variety of generic shapes and discuss how they relate to field observations. In Section 3.1, we test how various moulin shapes affect the equilibration timescales of the subglacial system using a constant meltwater input to the moulin. In Section 3.2, we test how the shape of a moulin affects its response to diurnally varying meltwater input. We conclude by interpreting our simulation results in the context of the englacial void ratio, bed connectivity, and consequent ice velocity.

2 Model description

Diameter-evolving subglacial channels have been simulated in numerous prior studies (e.g. Röthlisberger, 1972; Schoof, 2010; Spring & Hutter, 1981) and can be coupled with a reservoir to include the storage of the moulin (Clarke, 1996; Covington et al., 2012; Werder et al., 2010). This type of model provides a simple and efficient physically based framework for studying the dynamics of an individual moulin-fed subglacial channel.

To explore the relationship between moulin shape and moulin water level variation, we employ a simplified model of the coupled englacial-subglacial hydrological system. The model contains a single subglacial channel that is fed by a vertical moulin (Figure 1a). The moulin collects meltwater input which is then evacuated through a subglacial channel. The moulin's shape remains fixed throughout any single model run, with only the subglacial channel's cross-sectional area (S) allowed to evolve through melt and creep (Figure 1c), which are functions of subglacial discharge and effective pressure, respectively. Discharge and effective pressure vary with the height of the water column within the moulin's shaft, which we represent as hydraulic head (h). The rate of change of head (dh/dt) depends on the difference between the discharge into (Q_{in}) and out of (Q_{out}) the moulin and the storage volume within the moulin. Importantly, storage is controlled by the cross-sectional area of the moulin at the water level, $A_{\mathrm{r}}(h)$.

For this study, we implement the reservoir constriction model described in Covington et al. (2012) with the subglacial channel evolution model described in Schoof (2010), without the cavity component, as we assume the subglacial system is already channelized. The moulin component was adapted to allow the moulin cross-sectional area (A_{r}) to vary with depth. The model is composed of two coupled differential equations simulating the time evolution of moulin head (h) and the subglacial channel cross-sectional area (S) at the entrance of the channel where the water exits the moulin. The rate of change of head (h) within the moulin is given by

$$\frac{dh}{dt} = \frac{1}{A_{\mathrm{r}}(h)} \left(Q_{\mathrm{in}} - Q_{\mathrm{out}} \right), \tag{1}$$

where $A_{\mathrm{r}}(h)$ is the cross-sectional area A_{r} of the moulin at h, Q_{in} is the meltwater input into the moulin, and Q_{out} is the subglacial channel water output. Following Schoof (2010), we invoke the Darcy-Weisbach law,

$$Q_{\mathrm{out}} = C_3 S^{5/4} \sqrt{\rho_{\mathrm{w}} g h / L}, \tag{2}$$

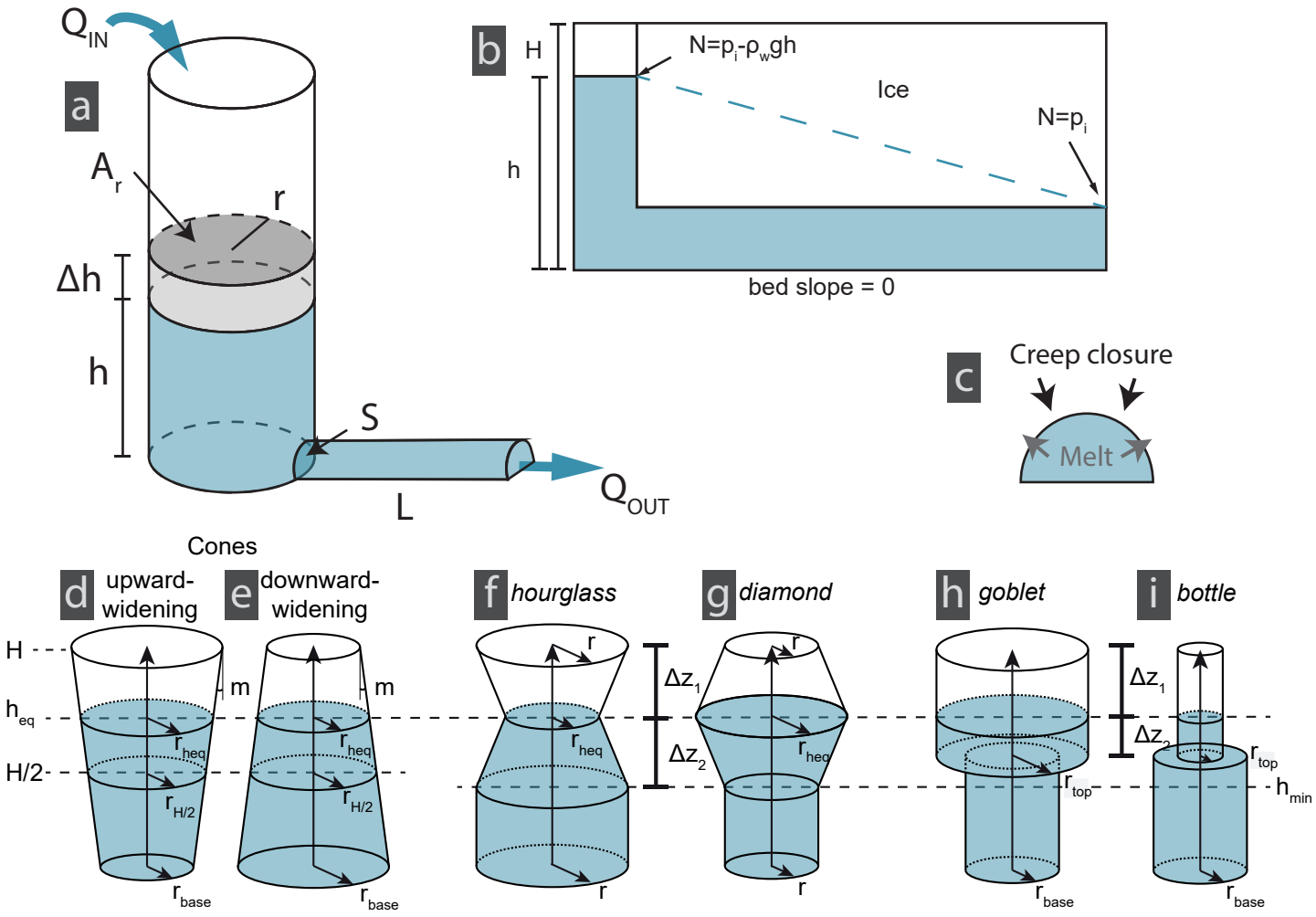

Figure 1. Schematic model diagrams. (a) Sketch of the model representing a moulin connected with a subglacial channel (Covington et al., 2012), with the meltwater input (Q_{in}), discharge (Q_{out}), moulin cross-sectional area (A_{r}), moulin radius (r), moulin head (h), subglacial channel length (L), and subglacial channel cross-sectional area (S). (b) Longitudinal cross-section of the model. The effective pressure (N) in the conduit at any point is the pressure of the ice (P_i) minus the hydraulic head ($\rho_{\mathrm{w}}gh$) defined with the water density (ρ_{w}), the gravity (g) and the head (h) relative to the bed. The blue dashed line represents the position of the water if we drilled a well in the subglacial channel. (c) The subglacial channel can creep closed or open depending on head and ice thickness adapted from (Schoof, 2010) (d-e) Cone-shaped moulins used for constant meltwater input simulations. We compare different cones by fixing the radius at the equilibrium head (h_{eq}) or at half of the ice thickness ($H/2$). The slope of the moulin wall is determined by m and is described in more detail in Supporting Text S2. (c-f) Moulin shapes used for the oscillating meltwater input simulations. We design the change in wall slope to be fixed at h_{eq} in (f) and (g), with Z_{hmin} just below the lowest water level in the set of simulations. The abrupt changes in radius in (h) and (i) are set to be between Z_{hmin} and Z_{heq}.

where L is the channel length or, equivalently, the distance between the moulin and the ice-sheet margin for this simplified case of a single subglacial conduit. The variable ρ_w is the water density, g is the gravitational acceleration, and the flux parameter $C_3 = 2^{5/4}\sqrt{\pi}\ /(\pi^{1/4}\sqrt{\pi+2}\sqrt{\rho_\mathrm{w} f})$, where f is the Darcy-Weisbach friction factor. The coupled subglacial channel creep and melt equations are based on the Röthlisberger (1972) and Nye (1976) description of R-channels and are given by

$$\frac{dS}{dt} = C_1 C_3 S^{5/4} \left(\frac{\rho_\mathrm{w} g h}{L}\right)^{3/2} - C_2 (P_i - \rho_\mathrm{w} g h)^n S, \tag{3}$$

for the melt opening parameter $C_1 = 1/(\rho_\mathrm{i} L_f)$, where L_f is the latent heat of fusion and ρ_i is ice density. The viscous creep closure parameter is $C_2 = Bn^{-n}$, where B is the Glen's law fluidity coefficient and n is the Glen's law exponent. The ice overburden pressure is $P_\mathrm{i} = \rho_\mathrm{i} g H$, where H is the ice thickness.

The model makes the following assumptions (Figure 1: (1) bed slope is zero; (2) the hydraulic gradient in the conduit is controlled by the large-scale ice sheet topography; and (3) melt and creep dynamics within the channel are controlled by the water pressure and ice thickness in the vicinity of the moulin; (4) water flow in the subglacial channel is turbulent; and (5) water that enters the moulin leaves only through the subglacial channel. For simplicity, we consider that all of the water transits through the channel; we do not account for loss or exchange of water with the distributed or weakly connected parts of the subglacial system. The model is a 0-D or lumped model, therefore, the cross-sectional area of the subglacial channel is represented by a single value.

While our model is a simplification of one part of the full subglacial hydrological system, it contains all of the components required to explore relationships between moulin storage and pressure variability within a subglacial channel without introducing unnecessary complexity and uncertain parameters. A variety of similar lumped models have been used in previous studies (Arnold et al., 1998; Bartholomew et al., 2012; Clarke, 1996; Covington et al., 2012, 2020; Cowton et al., 2016; Dow et al., 2014; Schoof, 2010; Stubblefield et al., 2019; Werder et al., 2010). Specifically, Stubblefield et al. (2019) demonstrated that such a lumped model displays very similar dynamics to a more complex extended channel model. We also test this assumption with a simulation comparing our simple 0-D model to an extended 1-D conduit model (supporting Text S3 and Figure S6). Limitations of our simplified modeling approach are discussed in more detail in Section 4.2.

2.1 Model setup

We use meltwater input rates in the range of estimated supraglacial stream discharges in the ablation zone on the western flank of the Greenland Ice Sheet (Smith et al., 2015). We run two broad classes of simulations. In the first set of simulations (Section 3.1), the meltwater input Q_{in} is fixed at $3\,\mathrm{m}^3/\mathrm{s}$ to test the equilibration of the subglacial system in the case of and abrupt change in meltwater input conditions, free of the diurnal variations typical of field-observed supraglacial discharge, to isolate the internal system dynamics from any effects of time-varying forcing. In the second set of simulations (Section 3.2–3.3), we use diurnally varying supraglacial meltwater input:

$$Q_\mathrm{in}(t) = Q_\mathrm{a} \sin(2\pi t/P) + Q_\mathrm{mean}, \tag{4}$$

where Q_in is meltwater input rate in function of time (t). Q_in oscillates around a mean meltwater input $Q_\mathrm{mean} = 3\,\mathrm{m}^3/\mathrm{s}$ with an amplitude (Q_a) of $0.4\,\mathrm{m}^3/\mathrm{s}$ and a period (P) of one day. This diurnal range of moulin input is kept low to prevent the simulated water level from overflowing. The simulations are run for an initialization period of 40 days, until the amplitude of the daily oscillations stabilizes. This allows us to isolate the dynamics created by varying meltwater input, rather than the damped oscillations produced during the equilibration of the system.

For most of the simulations (Section 3.1.1, 3.2 –3.3), we use a single ice thickness of 1000 m, which is appropriate for a moulin 30 km away from the margin, to simulate moulins located within a single area of the ice sheet. We choose parameter values that are roughly representative of the field areas in Greenland where moulin water-level data are available (Andrews et al., 2014; Covington et al., 2020). By keeping the ice thickness constant across simulations, we are able to isolate the influence of different moulin shapes and meltwater input magnitudes on moulin water level and subglacial water pressures. For the simulations in Section 3.1.2, however, we test how the system behaves at different positions across the ice sheet. In order to scale the ice thickness at the moulin to a series of conduit lengths representative of the profile of a land-terminating glacier in Greenland, we use an idealized square root glacier (Hewitt et al., 2012), with zero ice thickness at the margin and 1000 m ice thickness at 30 km from the margin, defined by

$$H = 1\,\mathrm{km}\sqrt{\frac{\mathrm{L}}{30\,\mathrm{km}}}, \tag{5}$$

where H is the ice thickness and L is again the subglacial channel length, equivalent to the distance between the moulin and the margin. This equation provides a single value of ice thickness in the vicinity of the moulin for each simulation with a given distance from the margin.

To explore the influence of moulin shape on subglacial water pressure dynamics, we use a series of idealized moulin shapes with geometries illustrated in Figure 1d–i. These shapes were chosen to cover a wide spectrum of possible moulin geometries because, to date, shapes of Greenland moulins in the region of summer water level fluctuations have not been mapped. We adapt the model of Covington et al. (2012) (Figure 1) by implementing a moulin with circular cross-sectional area with a depth-dependent radius (Clarke, 1996; Werder et al., 2010). We assume that the moulin has a circular cross-section and calculate the cross-sectional area $A_\mathrm{r} = \pi r^2$, for a depth-dependent radius r. The slope of the wall (m) is defined as $m = dr/dz$, where r is the moulin radius and z the elevation from the bed. The elevation difference Δz is calculated above the equilibrium head.

For specific simulation subsets, we compare moulins of different sizes and shapes with identical radii at either at the elevation of half of the ice thickness ($H/2$) or at the equilibrium head (h_eq). The equilibrium head (Röthlisberger, 1972) is introduced in Section 3 and is the altitude at which the water level in the moulin oscillates around, or stabilizes to, after a change in forcing. For the fixed meltwater input simulations (Section 3.1), we compare cone-shaped moulins (Figure 1d–e) of different sizes and shapes but identical radii at h_eq or identical radii at $H/2$. The parameterization is described in Supporting Text S2. For the oscillating meltwater input simulations (Section 3.2), we compare hourglass, diamond, goblet, and bottle-shaped moulins (Figure 1f–i). The parameterizations of moulin shapes are described in the Supporting Information (Figure S5).

3 Model experiments

3.1 Model experiments with a fixed meltwater input

For a fixed rate of meltwater discharge within a subglacial channel, there exist equilibrium values for head (h_eq) and channel diameter that can accommodate this discharge while simultaneously balancing the rates of wall melt and creep closure within the channel (Röthlisberger, 1972). If a channel is initialized at this state, then it will remain at equilibrium until the external forcing changes. When a subglacial channel is coupled to an englacial storage element, such as a moulin, the system can spontaneously oscillate around these values of equilibrium head and diameter, even with constant meltwater delivery (Clarke, 1996; Stubblefield et al., 2019). However, for the parameter space that we explore here, if our model is run with constant discharge and initialized sufficiently far from the equilibrium head and conduit diameter for that discharge, then it behaves

as a damped oscillator, which eventually approaches the equilibrium state (Supporting Figure S1). Therefore, the system exhibits two inherent timescales: one associated with the oscillation and one associated with the damping of the oscillations. We refer to the latter as the equilibration timescale. Effectively, the equilibration timescale approximates the time that is required for the system to evolve from one equilibrium state to another after a change in forcing, such as the moulin discharge.

Here, we run two sets of constant meltwater input simulations. In the first set, we fix parameters of ice thickness and channel length and explore the impact that moulin shape has on the equilibration timescale (Section 3.1.1). In the second simulation set, we systematically vary ice thickness and channel length for a subset of possible moulin shapes (Section 3.1.2). We use this second set of simulations to examine whether sensitivity to moulin shape varies across the ice sheet.

3.1.1 Effect of moulin shape on equilibration timescales

First, we examine the impact of moulin shape on equilibration timescale for fixed ice thickness and conduit length. We run four subsets of simulations using four different methods for varying moulin shapes. For the first subset, we use cylindrical moulins and simply vary the moulin radius from 5 to 15 m (Figure 2 a–c), which is in the range of radii observed in the field by (Covington et al., 2020). In the other three simulation subsets, we use moulins with sloping walls that widen either upward or downward. For the second subset, we employ a common moulin radius of 10 m at $H/2$ (Figure 2 d–f). For the third and fourth simulation subset, we fix the moulin radius to 10 m at h_{eq} (Figure 2 g–k). For the fourth simulation subset (Figure 2 j–k), however, we mirror the change in wall slope around h_{eq} so that the radius at h_{eq} is either the smallest or the largest within the range of water level oscillations. The wall slope, m, ranges from -2% to $+2\%$ for the simulations with a common radius at $H/2$, and from -6% to $+6\%$ for the simulations with a common radius at the equilibrium head elevation.

In the four sets of simulations shown in Figure 2, both head (h) and subglacial cross-sectional area at the moulin's outlet (S) have underdamped oscillations that reach an equilibrium head of about 750 m above the bed. For the cylindrical subset (Figure 2a–c), we observe that, for the same Q_{in} of $3\,\mathrm{m}^3/\mathrm{s}$, head oscillations in the larger moulin ($r = 15$ m) decay with an e-folding time of 13 days and have an oscillation period of five days, where the e-folding time is the time that it takes for the oscillation amplitude to decay by a factor of e. The e-folding time for the decay of oscillations in the smaller moulin ($r = 5$ m) is about one day with a oscillation period of less than two days (Supporting Tables S2–S4). This is consistent with common reservoir-model behavior, wherein the timescale for filling and draining increases with increasing reservoir size (e.g., Covington et al., 2009, 2012; Stubblefield et al., 2019).

In the simulation subset with cone-shaped moulins with radius fixed at $H/2$ (Figure 2d–f) the shapes and total volumes of the moulins are quite different than for the cylindrical cases. However, they display behavior that is similar to the cylindrical cases. For example, an upward-widening cone with wall slope of $+2\%$ from the vertical axis (purple line) has a low total storage capacity below the water line compared to a downward-widening cone with the opposite wall slope (-2%; red line). However, we observe very similar behavior in the time evolution of h and S as for cylindrical moulins, where equilibration time increases with moulin storage volume within the range of water level oscillation. We probe this further using the third and fourth subset of modeled moulins, where storage at h_{eq} is fixed with a radius of $r = 10$ m (Figure 2g–i and j–l). For the third subset (Figure 2g–i), we observe that the timescales of both oscillation and equilibration are nearly identical from one moulin to another, regardless of wall slope. This is true even for extreme cases of wall slope (Figure 2g–i, red and purple lines). Both h and S vary nearly identically as in the cylindrical (2c, black line) and cone $H/2$ (2f, black

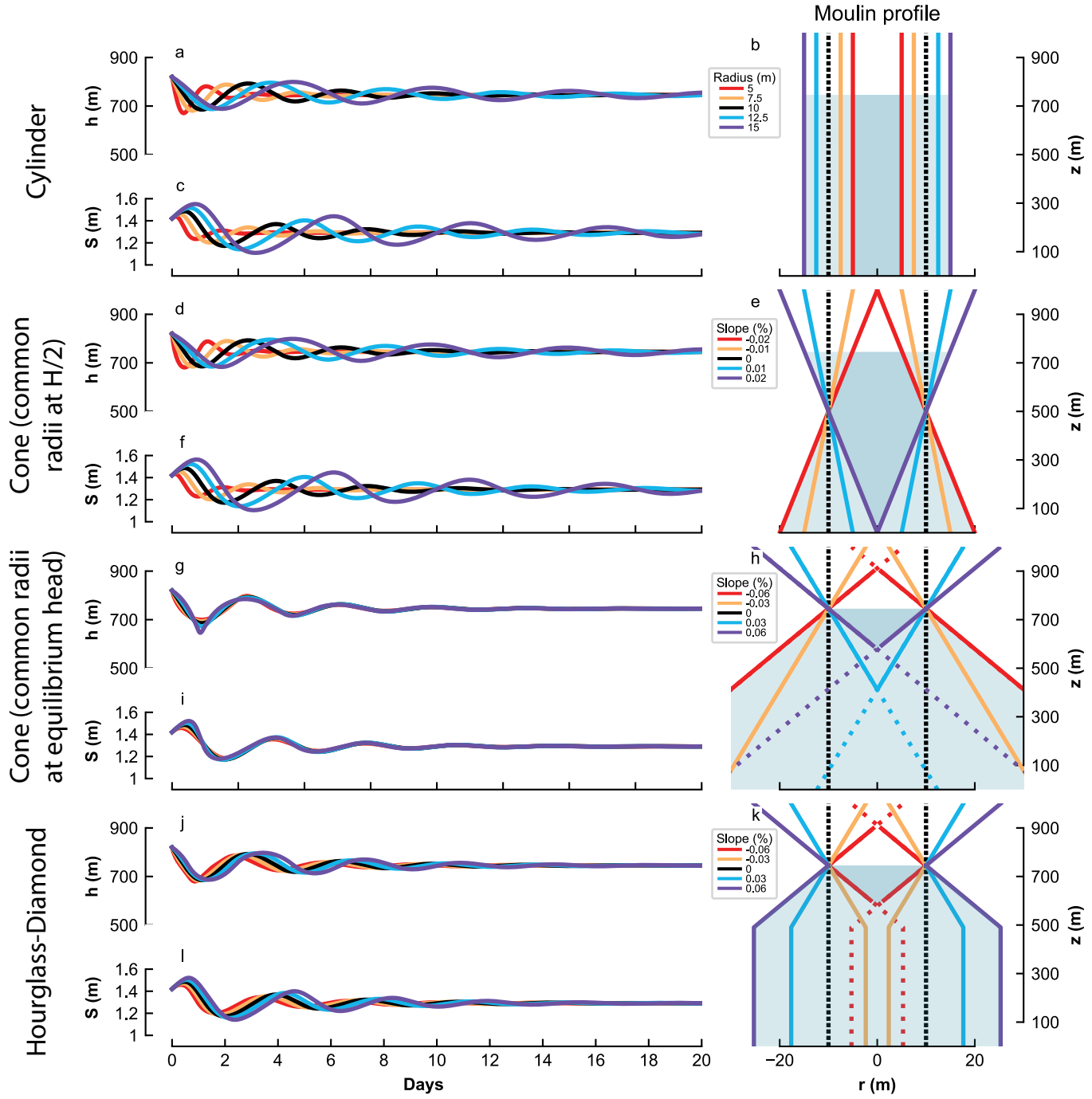

Figure 2. Equilibration timeseries of **head (h)** and **channel cross-sectional area (S)** simulated with a fixed meltwater input Q_{in} for various moulin shapes. For all simulations the length and thickness of the glacier is constant. Rows correspond to the following moulin shapes: cylindrical (a–c) with variable diameters, conical (d–i) with variable wall slopes with the radius held constant at an elevation of half the ice thickness (d–f) or at the equilibrium head altitude (g–i), and hourglass-diamond (j–l) centered around the equilibrium head altitude. For each shape, the timeseries of moulin head ($h(m)$) and subglacial channel cross-sectional area (S) are shown on the left. The moulin's cross-sectional profile is on the right with dark blue and light blue illustrating water common to all moulins and water in a subset of moulins, respectively. The vertical axes of moulin profiles are at scale with head, but not with S. Model parameters are $Q_{\text{in}} = 3\,\text{m}^3/\text{s}$, $L = 30\,\text{km}$, $H = 1000\,\text{m}$.

line) cases that have $r = 10\,\mathrm{m}$ at h_{eq}. We observe a similar behavior for the fourth subset (Figure 2j–l), with a bit more variation in the equilibration timescales between the different simulations than for the cone-shaped moulins. The mirroring of the slope above and below h_{eq} increases the effect of wall slopes, since the change in area is either positive or negative during both high and low water. For the conical moulins, the opposite signs of the changes in area above and below equilibrium have a cancelling effect.

While the dynamical timescales are effectively the same for all the simulations with similar $r(h_{\mathrm{eq}})$, the shape of the oscillations near the peaks and the troughs depends on wall slope (Figure 2g–h). The shape of the head extremum is rounder in Figure 2g (purple line) when the moulin widens in the direction of head displacement (red line), and more sharply peaked when the moulin narrows in that direction.

3.1.2 Equilibration timescales for different ice thicknesses

To examine if the equilibration timescale is sensitive to the moulin position on the ice sheet, we run a series of simulations for several positions along a profile of an idealized parabolic glacier (Figure 3) by systematically varying the parameters of H at the moulin and L from the moulin to margin. As before, each of these simulations uses a single ice thickness representative of the ice thickness near the moulin. The idealized glacier shape is only used to appropriately scale ice thickness at the moulin with distance from the margin. We use the same four classes of moulin shapes as in Section 3.1.1. For each shape class we compare the oscillation timescale (τ_{osc}), which represents the period of the underdamped fluctuations, and the damping timescale (τ_{damp}) which is the e-folding time over which the system equilibrates. We extract τ_{osc} and τ_{damp} of h and S by fitting the solution for a damped harmonic oscillator to our simulated timeseries (Supporting Figure S1), using

$$h(t) = a e^{-t/\tau_{\mathrm{damp}}} \sin\left(\frac{2\pi}{\tau_{\mathrm{osc}}} t + \phi\right) + h_{\mathrm{eq}} \tag{6}$$

$$\phi = \begin{cases} \pi & \text{if} \quad h(t=0) < h_{\mathrm{eq}} \\ 0 & \text{if} \quad h(t=0) > h_{\mathrm{eq}} \end{cases} \tag{7}$$

where a is the amplitude, t is time, and ϕ is the phase shift of the simulated timeseries.

For cylindrical moulins with the same meltwater input (Q_{in}), we find that oscillation and damping timescales (τ_{osc} and τ_{damp}) increase with distance from the margin and with increasing radius (Figure 3, first column). Note that τ_{osc} in (Figure 3e–h) has high values close to the margin, where the damping of the head towards equilibrium is quicker than a full period of oscillation. Consequently, our fitting method for finding the equilibration timescales is likely less accurate close the margin. For cone-shaped moulins with common radii at $H/2$ (Figure 3, second column), the timescales display an intersection point around 10 km from the margin, a distance that is specific to our parameter choices. Here, for downward-widening moulins, the timescales initially decrease with distance from the margin, because increases in the equilibrium head bring the water levels into a narrower portion of the moulin. For upward-widening moulins a similar, but opposite, effect enhances the increases in the timescales with distance from the margin. As a result, τ_{damp} for a wall slope of 0.02 reaches a maximum of 15 days at 40km, where the moulin radius at the water level becomes disproportionately large compared to the meltwater input. Overall, these results illustrate that the diameter of the moulin at h_{eq} is the primary control on these timescales and that ice thickness has a secondary effect. This is further demonstrated by the simulations for cone-shaped and diamond-hourglass moulins with common radii at h_{eq} (Figure 3 right columns) which show reduced variation in τ_{osc} and τ_{damp} across moulin shapes, so long as the radius at h_{eq} is the same.

For these simulations, both timescales reflect mainly the position of the moulin on the ice sheet, not the moulin shape. Furthermore, τ_{osc} and τ_{damp} for all cone-shaped moulins

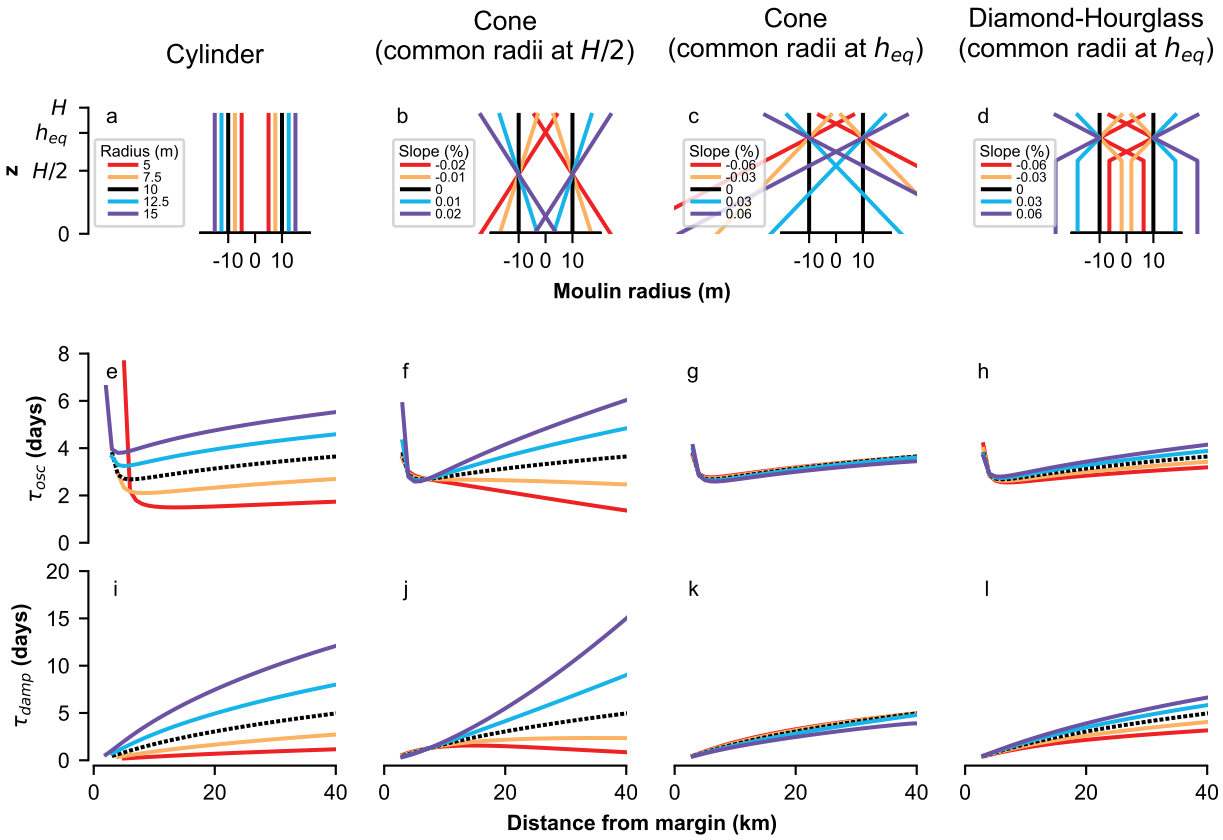

Figure 3. The equilibration timescales, along an idealized parabolic ice sheet profile (Equation 5) for cylindrical (a), conical (b–c), and hourglass-diamond (d) shaped moulins. The oscillation timescale (τ_{osc}) (e–h) represents the period of the underdamped fluctuations, while the damping timescale (τ_{damp}) (i–l) is the e-folding time over which the system reaches equilibrium. For a cylindrical moulin (left column), a cone-shaped moulins with a fixed radius at $H/2$ (second column) and at h_{eq} (third column), and diamond-hourglass shaped moulins with a fixed radius at h_{eq} (right column).

in this subset are the same as that of the cylindrical moulin with a radius of 10 m, which is equal to the radius of the cone-shaped moulins at h_{eq}. Therefore, we find that the moulin's cross-sectional area at h_{eq} controls the equilibration timescales.

3.2 Model experiments with an oscillating meltwater input

On glaciers and ice sheets, meltwater discharge flowing into moulins is not constant in time but oscillates with changes in surface melt. In this section, we focus on the impact of moulin shape on the dynamics of moulin water level and subglacial conduit cross-sectional area under diurnally varying meltwater delivery.

We test a variety of simple, physically plausible shapes. We design these moulins such that the changes in cross-sectional area are focused within the range of elevations of water level oscillation. This is because we observe in Section 3.1 that only changes in moulin shape around h_{eq} affect the head and subglacial channel size. We use two different approaches to vary moulin shape near h_{eq}. In the first approach, we vary the moulin wall slope around h_{eq} ("hourglass", "diamond", Figure 1f,g) to keep our focus on the wall slope and not on the change in cross-sectional area at h_{eq}. In the second approach, we abruptly change the moulin cross-sectional area at h_{eq} ("goblet", "bottle", Figure 1h,i) to mimic differential melting observed in moulins in the field. We compare results from all of these runs to the cylindrical standard, for a total of five moulin shapes.

As noted in Section 3.1, moulin shapes do not have a strong influence on equilibration timescales; however, moulin shape does affect the amplitude and shape of the peaks and troughs in head and subglacial channel cross-sectional area in response to oscillating meltwater input. In this simulation subset, we observe how the five tested shapes affect the amplitude and shape of the oscillating responses in h and S for the same sinusoidal meltwater input.

We compare cylindrical moulins, with radii varying from $3.5 - 15$ m (Figure 4a–e), to hourglass- and diamond-shaped moulins with different wall slopes but with a common radius at one position in the moulin (Figure 4f–o), and to moulins with fixed wall slopes with varying radius (Figure 4p–y).

For similar Q_{in}, the oscillation amplitudes of h and S are controlled by the moulin volume within the oscillation range, similar to what was observed with a fixed input (Section 3.1). The magnitude of A_r in the head oscillation range, whether depth-independent (Figure 4a–e) or depth-varying (Figure 4f–y), strongly affects the amplitude of oscillations. For a given A_r at h_{eq}, a wall slope of just -2% from the vertical axis (Figure 4f–j red) can double the oscillation amplitude compared to a cylinder. This is due to the depth-dependent moulin volume within the oscillation range: the ability of the moulin to store water decreases as h rises above h_{eq}, thus forcing a faster rise. This change in oscillation amplitude is particularly pronounced above the equilibrium head, where increases in radius at h_{eq} systematically reduce the amplitudes, regardless of the slope.

We observe asymmetry in both peak shape and the height of peaks versus depth of troughs above and below equilibrium. This asymmetry is driven by the asymmetry between the rates of melt and creep closure of the subglacial channel. In general, under conditions typical of an ice sheet, the subglacial channel is able to close faster than it can grow. This means that the subglacial channel closes quickly as meltwater input decreases and water pressure falls. But, when meltwater input increases, and the conduit must reopen, the melt opening process is slower. Accordingly, the water level increases faster than the conduit can accommodate, creating a large increase in water level in the moulin.

To investigate the relationship between moulin water level variation and moulin storage capacity, we use the dimensionless meltwater input frequency f^* from Covington

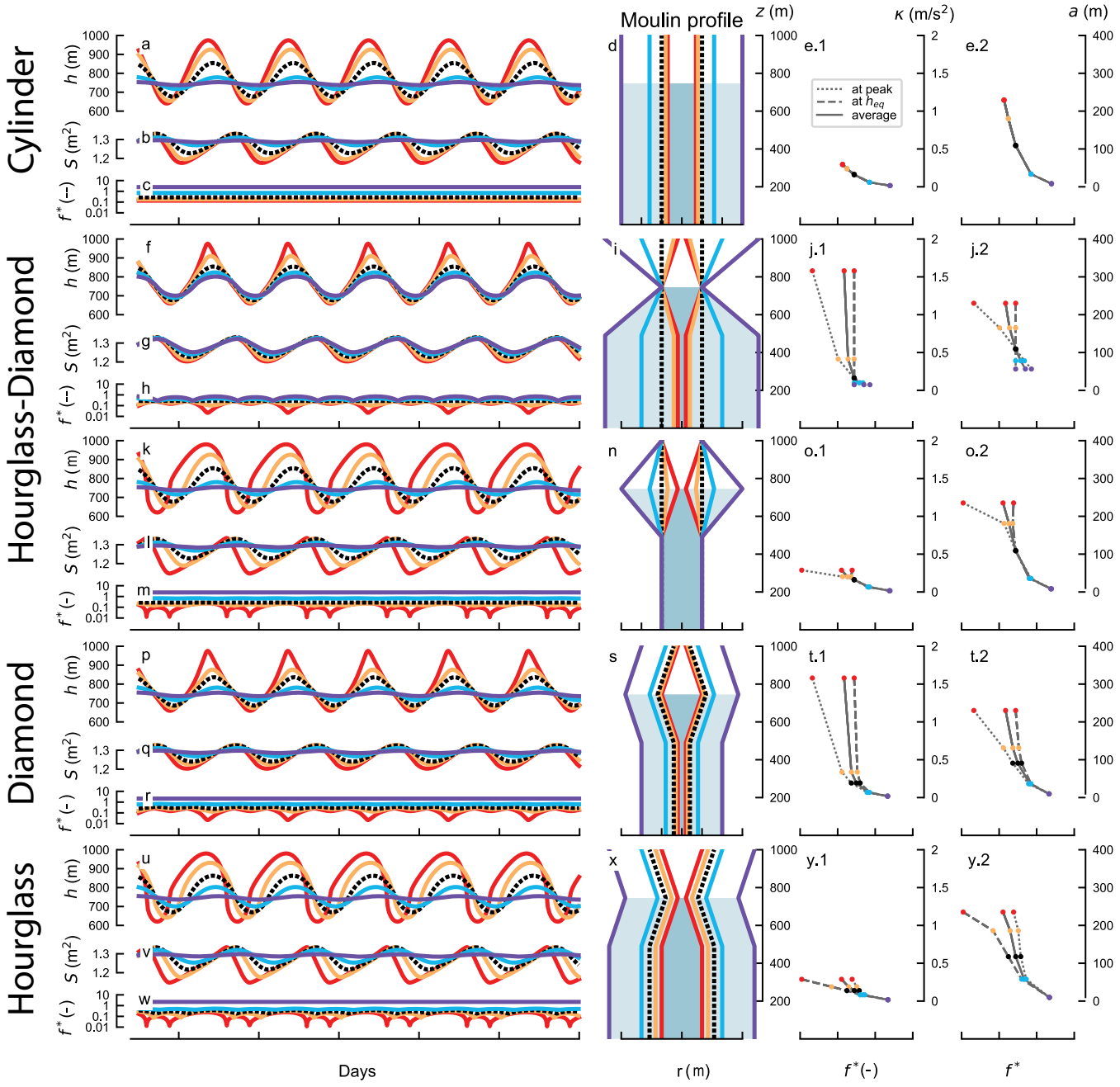

Figure 4. Timeseries of **head** (h), **channel cross-sectional area** (S), and **dimensionless meltwater input frequency** (f^*), for a **sinusoidal** Q_{in} oscillating from 2.6 to 3.4 m^3/s with a daily period for multiple idealized moulin shapes. For cylindrical moulins (a–e) the **radius** (r) is uniform such that a large radius dampens oscillations in h and S, reducing f^* uniformly. For hourglass-diamond shaped moulins the radius is either fixed at h_{eq}, with varying wall slope above and below h_{eq} (f–j), or the radius is fixed above and below the water oscillation, and the radius varies at h_{eq} (k–o). For diamond-shaped (p–t) and hourglass-shaped (u–y) moulins the slope is fixed and the radius varies between model runs. Moulin profiles follow Fig (3). The correlation between **peakedness,** κ—represented by the second derivative of the head oscillation—and f^* (left) and the correlation between the **peak-to-peak amplitude of oscillation** (a) and f^* (right) are shown for each moulin shape. Values corresponding to peak head (dash-dot), equilibrium head (dashed), and mean values (solid) are shown.

et al. (2020), which is the ratio of the time it takes for the moulin to fill to overburden pressure and the duration of the meltwater input cycle:

$$f^* = \frac{\tau_{fl}}{P_{osc}}, \tag{8}$$

where the period of oscillation of the meltwater input (P_{osc}) is one day and the storage timescale (τ_{fl}) is given by

$$\tau_{fl} = \left(\frac{\rho_\mathrm{i}}{\rho_\mathrm{w}}\right)\frac{HA_\mathrm{r}}{\overline{Q_\mathrm{in}}}, \tag{9}$$

where ρ_i and ρ_w are the density of ice and water, respectively, H is the ice thickness, and A_r is the moulin cross-sectional area. Essentially, a moulin acts as a low-pass filter, where water storage filters out frequencies above $f^* \gtrsim 1$. For the cylindrical case, where A_r is depth-independent, so too is f^* (Figure 4c). For non-cylindrical moulins, however, f^* changes with head (Figure 4h,m,r,w). For these cases, we use local cross-sectional area as a function of head, $A_\mathrm{r}(h)$, to calculate f^* as a function of head.

For a cylindrical moulin, we find that when $f^* > 1$ (Figure 4a–e, purple line), diurnal oscillations are almost completely filtered out, but they remain for $f^* < 1$ (Figure 4c). For the diamond-shaped moulin (Figure 4r, yellow and red) the timeseries of f^* shows two pointy troughs per 24h period. The large and the small f^* troughs coincide with the peaks and troughs, respectively, of h, where A_r reaches minima. The main trough is due to the narrowing above h_eq, and the secondary trough is due to the narrowing below h_eq. Even though the moulin shape is symmetric above and below h_eq, the water level rises higher above h_{eq} than it falls below, due to the asymmetry caused by subglacial melt-creep dynamics. For the hourglass shaped moulin, the twice-daily troughs in f^* coincide with the subglacial channel cross-sectional extremum (Figure 4w). In this case, the narrowest portion of the moulin is positioned at h_eq.

We hypothesize that variations in oscillation shape (amplitude and peakedness) are controlled by the dimensionless meltwater input frequency (f^*). To quantify the peakedness (κ) of the oscillations, we calculate the curvature of the timeseries in the vicinity of the peak, using

$$\kappa = \left.\frac{d^2h}{dt^2}\right|_\mathrm{peak}, \tag{10}$$

where larger curvature values will correspond to a sharper peak. Finally, we calculate the amplitude (a) of the oscillation above h_eq as

$$a = h_\mathrm{peak} - h_\mathrm{eq}. \tag{11}$$

To test our hypothesis, we compare values of f^* at h_eq (dashed lines), h_peak (doted-dashed lines), and averaged (solid) against κ and a (Figure 4e,j,o,t,y). It is important to keep in mind that for a specific H and Q_in, which here are held fixed, f^* is a direct reflection of A_r. We find that the smallest value of f^* within the head oscillation range controls the amplitude of oscillations if $f^* < 1$ (Figure 4), while the peakedness is controlled by f^* averaged (Figure 4p–t, red line). Additionally, when the trough in f^* corresponds to the equilibrium head (Figure 4h–y, red line), we observe deformation of the head oscillation shape, but not a significant increase in κ. When the minimum values of f^* coincide with a head maximum or minimum, the shapes of the peaks and troughs become distorted. In other cases, when the troughs in f^* coincide with the water level being at h_eq, then the shape distortion appears around the mean of the oscillation (Figure 4k–m, red line).

3.3 Effect of abrupt change of moulin shape

Next we investigate how an abrupt change in moulin shape at a prescribed depth affects the oscillation dynamics. Field exploration of moulins in Greenland (Covington

et al., 2020; Reynaud & Moreau, 1994; Moreau, 2009) has found ledges in some moulins, or large subaerial volumes that narrow at the water line. To represent these moulins simply, we design goblet and bottle-shaped moulins that comprise two stacked cylinders of different radii (Figure 5f–j). We use these moulins to explore a hypothetical large change in volume above h_{eq} or just below the lowest head (Figure 5k–o).

First, we test how the equilibration timescales are affected by an abrupt change in shape. In contrast to the lack of impact of moulin wall slope (Figure 2g–i), we find that abrupt enlargement or reduction of moulin size at h_{eq} substantially changes the oscillation and damping timescales for the same meltwater input. We find that bottle-shaped moulins have faster equilibration timescales than cylindrical moulins, while hourglass-shaped moulins require more time for the head to equilibriate (Supporting Figure S3).

We also test how this abrupt change in volume affects the head oscillations with diurnally varying meltwater input (Figure 5). We find that abrupt changes in moulin radius around h_{eq} affect the amplitudes of the oscillations in h and S. This is despite the fact that all moulins had an identical radii for some 60% of the depth. An increase of the moulin radius by just one meter (10%) reduced the amplitude of the water oscillations by a third (Figure 5f–j, black and blue lines), suggesting that strongly dampened water level oscillations can occur in moulins with a wide chamber above the water line, regardless of their shape below the water line. In contrast, goblet and bottle-shaped moulins in which the cylinders of different radii join below the oscillation range (Figure 5k–o) do not show variations in the pattern or amplitude of water oscillation. These final simulations illustrate that water level oscillations are insensitive to static storage volumes that are always below the water level.

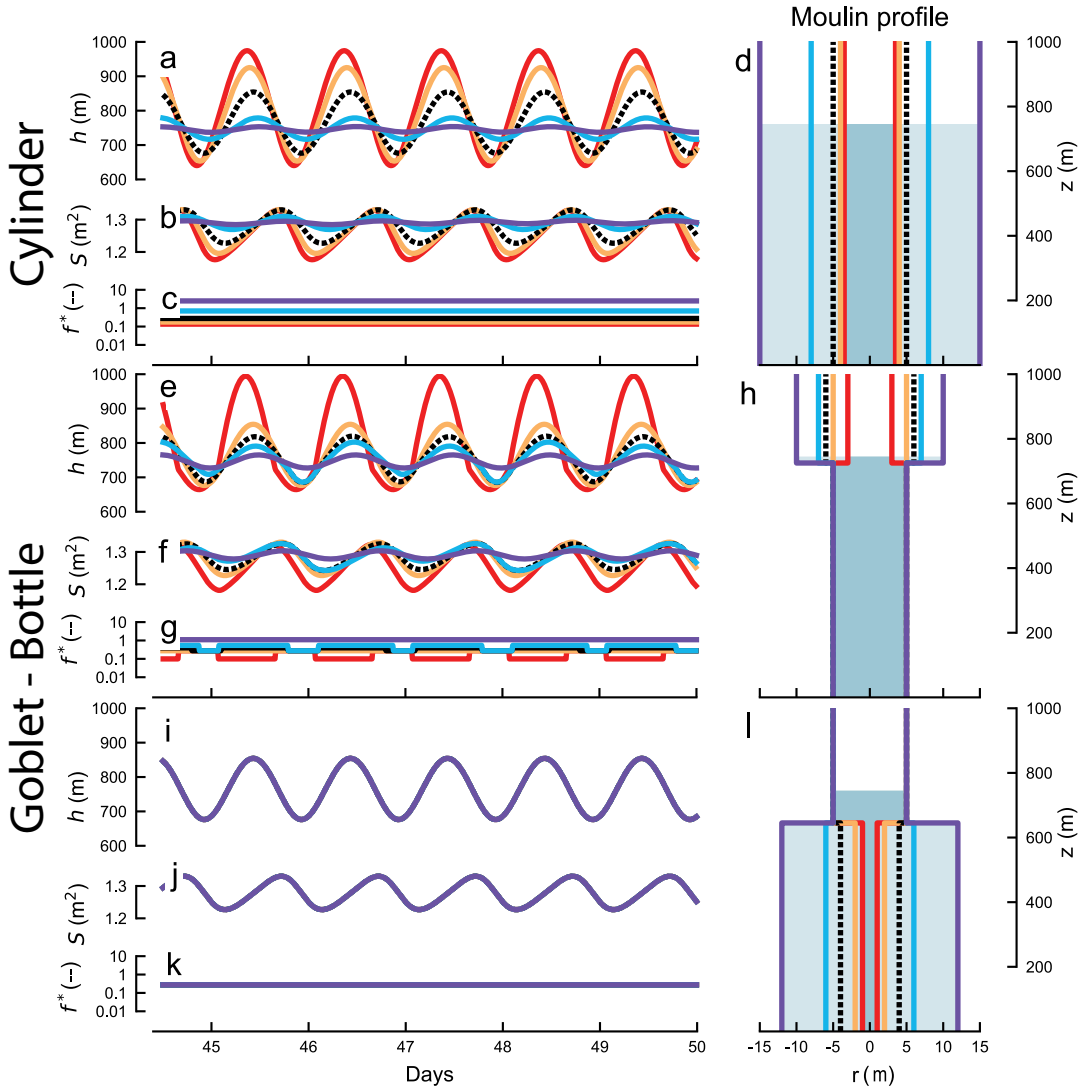

Figure 5. Timeseries of **head (h)**, **channel cross-sectional area (S)**, and **dimensionless meltwater input frequency (f^*)**, for a daily **sinusoidal** Q_{in} oscillating from 2.6 to 3.4 m^3/s for multiple idealized moulin shapes: Cylindrical (a–d), goblet-bottle-shaped with radius fixed below (e–h) and above (i–l) the equilibrium head (h_{eq}).

4 Discussion

4.1 Controls on head variability

Moulin storage modulates changes in subglacial pressure by regulating variations in moulin hydraulic head (Andrews et al., 2021; Covington et al., 2012, 2020). Here, we examine how vertical changes in moulin storage impact the amplitude and form of moulin head oscillations. Moulins act as low-pass filters between meltwater inputs at the surface and englacial discharge into the subglacial system, removing high-frequency oscillations and transmitting low-frequency oscillations. This low-pass filter behavior can be quantified using the dimensionless oscillation frequency, f^*, where oscillations that occur on timescales where $f^* \gtrsim 1$ will be strongly damped.

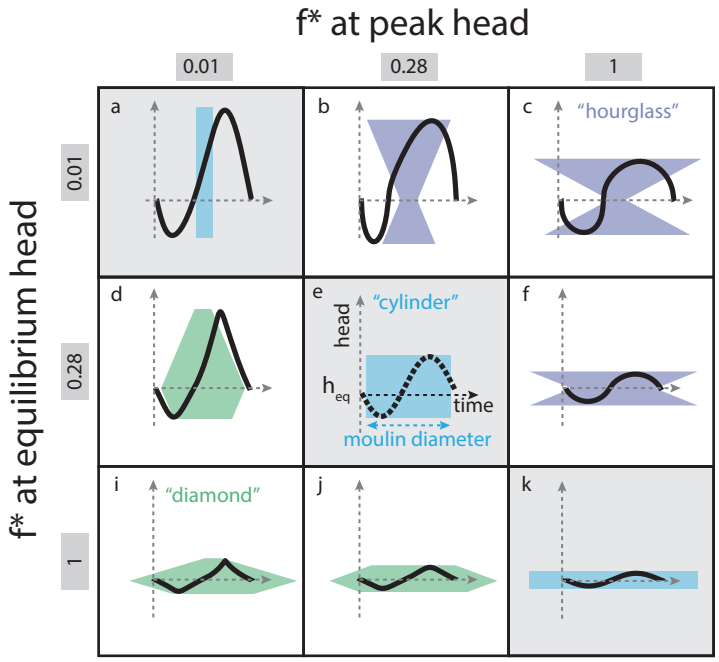

Figure 6. The amplitudes and shapes of moulin head (h) oscillations for selected dimensionless meltwater input frequency (f^*) at peak head (h_{peak}) and at equilibrium head (h_{eq}). Black lines show a single period of head oscillation. Blue shading shows the moulin shape within the range of water level oscillation. Moulin shapes are scaled consistently against the head timeseries and with one another. All moulin shapes are symmetric about h_{eq}. Values of f^* are highlighted in grey.

The storage that impacts the head oscillations in the moulin is the storage within which the head varies. We define "dynamic storage" as the storage that is filling and draining, and "static storage" as the storage that is always full of water. Note storage that is static at the daily timescale could be dynamic at a longer timescale. The impact of dynamic storage on the water level patterns that we observe can be categorized using the values of f^* at the equilibrium head elevation, $f^*(h_{\mathrm{eq}})$, and at the peak head elevation, $f^*(h_{\mathrm{peak}})$. We generalize these patterns of behavior in Figure 6, where we display selected 24 h head oscillations for specific choices of $f^*(h_{\mathrm{eq}})$ and $f^*(h_{\mathrm{peak}})$.

Cylindrical moulin cases are depicted along the diagonal of Figure 6(a,e,k), where one can see the effect of increases in dimensionless meltwater input frequency leading to decreases in oscillation amplitude. However, oscillation amplitude also decreases if mov-

ing along an axis of increasing $f^*(h_{eq})$ or increasing $f^*(h_{peak})$ (Figure 6b,c,f), suggesting that average f^* within the range of oscillation is responsible for controlling amplitude. The peakedness of moulin head oscillations is controlled by whether f^* decreases or increases as the water level approaches a peak or trough. Diamond-shaped moulins, which fall below the diagonal in Figure 6, and have $f^*(h_{eq}) > f^*(h_{peak})$, produce sharply peaked oscillations. Hourglass-shaped moulins, which are located above the diagonal in Figure 6, and have $f^*(h_{eq}) < f^*(h_{peak})$, produce rounded oscillations. For the diamond-shaped cases, cross-sectional area decreases towards the peaks and troughs. These decreases in A_r drive an increase in the rate of change in head, leading to sharpening of the peaks. Similarly, if A_r increases towards peaks and troughs, then the rate of change in head will be reduced near peaks and troughs, producing rounded peaks. In addition to the low-pass filter behavior of moulins, changes in storage with depth can alter the temporal shapes of water level oscillations. Therefore, it may be possible to constrain the shapes of moulins by using a timeseries of moulin water levels observed in the field.

4.2 Influence of model assumptions on simulation results

The simplification of the subglacial channel model to an ordinary differential equation is based on the assumptions that (1) the hydraulic gradient is set by the large-scale topography of the ice sheet, which can be approximated by h/L, and (2) that changes in flow resistance are controlled by the cross-sectional area of the subglacial channel near the moulin. The first assumption is based on the long and relatively flat topography of the ice sheet, and the fact that the hydraulic grade line within subglacial conduits tends to roughly follow the glacier topography (Röthlisberger, 1972). The second assumption is based on the idea that the largest variations in water flow resistance in the subglacial channel occur near the moulin, because the ice is thickest there and the discharge fluctuations are the largest. In a recent lake drainage modeling study, Stubblefield et al. (2019) demonstrated that the usage of simplified coupled ordinary differential equations (ODEs), similar to the ones we use, instead of more complex partial differential equations (PDEs), is sufficient for simulating pressure dynamics, while saving considerable computing time and reducing parameter complexity.

We also compared the outputs from a more complex PDE model, where the channel can evolve along the horizontal axis, against our lumped ODE model (Supporting Text S3 and Figure S6). We found that using the more complex model did not significantly change the water level dynamics (less than 10% of the ice thickness). However, the mean water level is somewhat different in the two simulations, a result of the simplifying assumptions in our ODE model. In the ODE model, the hydraulic gradient is likely to be a bit steeper than it would be in reality, effectively increasing the flow for a given hydraulic head and conduit cross-sectional area, S. On the other hand, the average S is likely to be underestimated, as we use a value representative of where the ice thickness is the largest. In reality, we expect S to increase as the ice thickness decreases along the conduit toward the margin. The smaller S in our ODE model would effectively decrease flow for a given hydraulic head, somewhat countering the influence of the other assumption. However, these two effects do not quite balance, resulting in the slight differences in mean head values in the discretized (PDE) and lumped (ODE) conduit models. However, as we are interested in the relative change in water level induced by different moulin shapes, rather than the absolute head values, the simplified representation of the subglacial conduit in our model does not have a substantial influence on our conclusions.

A second important simplification of the model is that it does not have a distributed network, which in reality could exchange water with the subglacial channel. We might expect such exchange flows with a distributed network to reduce the amplitude of oscillation of the head in the moulin. However, observed water levels in moulins in Greenland rarely reach pressures observed in the unchannelized portion (Andrews et al., 2014;

Covington et al., 2020; Mejia et al., 2021; Meierbachtol et al., 2013; Wright et al., 2016), which is necessary for the water to be pushed into the distributed network. Furthermore, daily changes in storage volumes within the distributed network are limited, again suggesting that they would not have a substantial impact on moulin water level dynamics (Covington et al., 2020).

Arguably, one of the most limiting assumptions in our model is its representation of the englacial–subglacial system as a single moulin connected to a single channel, rather than a network. In reality, moulins will interact with other nearby moulins, such that the shape of a single moulin will not be the only driving factor of head variation (Andrews et al., 2014, 2021). Moulin water level dynamics will likely average over storage available in nearby moulins that are tightly coupled through the conduit network. Also, we might expect some background discharge from other moulins or basal melt that could provide a baseflow discharge that reduces oscillation amplitude (Andrews et al., 2021; Trunz, 2021). While such effects are likely to influence moulin water level dynamics in nature, the model presented here is sufficient to explore the relative impact of moulin shape on the amplitude of oscillation.

4.3 Potential shapes of Greenland Ice Sheet moulins

Here we have used idealized shapes to explore, in general, how moulin shape can influence subglacial water pressure dynamics. However, real-world moulins are likely to display a somewhat narrower range of shapes than we modeled. In general, moulins will evolve through a combination of melt due to turbulent flow of water and viscous and elastic deformation of the ice (Andrews et al., 2021; Catania & Neumann, 2010; Poinar et al., 2017). Is it not clear, however, whether moulins often evolve to an equilibrium form or whether moulin lifetimes are sufficiently short that they are abandoned before the drivers of expansion and contraction can reach a balance. However, the size of a moulin should be correlated to the size of the supraglacial stream feeding it. This likely restricts plausible ranges of f^*, which depends linearly on moulin volume and inversely on meltwater discharge.

The limited field observations inside the Greenland Ice Sheet (Covington et al., 2020; Reynaud & Moreau, 1994) have not yet extended beyond the upper 10–20% of the ice thickness, because moulins have been water filled below that depth at the time of exploration. Water levels in the fall, when exploration is possible, may also be somewhat higher than average summer water levels and geometries may be modified due to the increased creep closure rates. Some observed moulins also have ranges of water level oscillation that are much larger than the explored thicknesses (Andrews et al., 2014), highlighting additional uncertainty on moulin shapes within the relevant range of water level oscillations. Nevertheless, observations in the upper parts of moulins suggest that goblet shapes may be more plausible than bottle shapes. Some explored moulins are roughly cylindrical with a reduction of diameter at the water line, as observed in a moulin nearby the the FOXX moulin (monitored by Andrews et al. (2014) and explored by Covington et al. (2020)) and in the Isortoq moulin (Reynaud & Moreau, 1994). Phobos moulin was roughly goblet-shaped, with a large chamber just above the water level (Covington et al., 2020). We use the bottle shape moulin here as an end-member case to understand how head dynamics relate to moulin shape, but it is unclear what physical processes could produce such a shape. Phobos moulin did narrow substantially near the ice surface, but it is unknown whether water levels would ever reach that elevation because the water level measured in the nearby Radical moulin remained below 225 meters depth (Covington et al., 2020) throughout the 2017 melt season.

Goblet-shaped moulins could be produced by differential melting of the walls, with more melt above the equilibrium water level than below, or by strong creep closure of the ice at depth. Field observations show that moulins tend to form in pre-existing crevasses

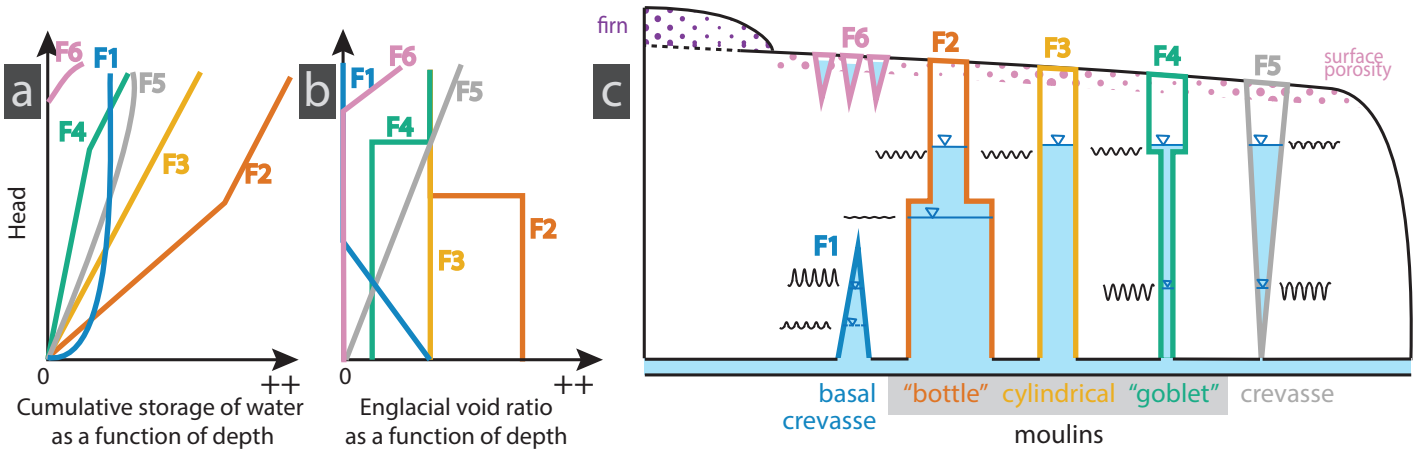

Figure 7. Conceptual sketch of englacial storage and englacial void ratio as a function of depth for idealized moulin shapes. The total stored water (a) gradually increases with increases in head, while the englacial void ratio (b) only changes when the radius of the moulin changes. (c) Representations of moulin profiles plotted in (a) and (b). Black oscillating timeseries depict the amplitude of water level oscillations in moulins when the water is at a specific depth. Oscillation amplitude is not a function of total moulin/englacial storage, but the dynamic storage, which is localized within the range of head oscillation.

or shear fractures (King, 2018; Smith et al., 2015). Such crevasses or fractures could also create zones of preferential melt, wherein waterfall erosion processes and supraglacial stream knickpoints could more rapidly enlarge moulin cross-sections. Because creep closure is relatively slow in the top 100 meters of an ice column, these goblet shapes should tend to be available for reuse from year to year (Catania et al., 2008). It is unclear if reused moulins provide more storage than newly formed moulins, as the moulin partially creeps closed at the end of the melt season. More field observations and modeling are necessary to fully understand the processes that control moulin shapes.

4.4 Implications for large-scale glacier hydrological models

To more accurately simulate subglacial pressure amplitudes in the efficient portion of the subglacial drainage system, subglacial hydrological models often use an englacial void parameter. The englacial void parameter accounts for the transient storage of water in the englacial system (Flowers & Clarke, 2002). Englacial storage of water connected to the bed will influence the amplitude and the timing of peak subglacial water pressure. Moulins may be the most important englacial storage component, as they are directly connected to both the subglacial and supraglacial channels (Covington et al., 2020). The englacial void ratio or englacial void fraction parameter, is typically calculated as the volume of void space divided by the volume of ice (Downs et al., 2018; De Fleurian et al., 2018; Flowers, 2015). Although overall storage in the glacier is important on longer timescales, we find that it is only the storage or englacial void ratio within the head oscillation range, which we call the dynamic storage, that affects the water level dynamics in the efficient portion of the bed on a daily timescale.

As we find that the head oscillation amplitudes are strongly affected by dynamic storage, we reflect here on the extent to which different types of englacial storage contribute to this dynamic storage. We compare five shapes to illustrate how total water storage and local englacial storage vary with depth (Figure 7, englacial storage elements

are numbered from F1 to F6). Moulins sketched in Figure 7(F2–F4) show that even though they have very different total storage capacities, they could induce similar head oscillation ranges if the water level is close to their tops (upper sinusoids). In the case of much lower water levels, though, the moulins would create very different oscillations (lower sinusoids). The high dynamic storage in moulin F2 will dampen oscillations, whereas the low dynamic storage in moulin F4 will enable large oscillations. Crevasses (Figure 7-F5) connected to a moulin (Colgan et al., 2011) could provide a substantial extra volume that could dampen oscillation amplitudes and filter out high frequency variation. Without such a connection, crevasses could provide long term storage at seasonal timescales (McGrath et al., 2011). Basal crevasses (F1 in Figure 7), if they are connected to the channelized system, would only influence the oscillation dynamics if the water level was below the top of the crevasse. They have been found in drilling (Harper et al., 2010) and seem to be present when basal water pressures are above overburden pressure (van der Veen, 1998). Therefore, they may be more likely in the weakly connected portion of the bed that has higher water pressure than the channelized system (Andrews et al., 2014; Wright et al., 2016). The firn aquifer, the surface crevasses, and the porosity at the surface (F6), while they could delay the arrival of meltwater to the moulin, are storage elements that are completely decoupled from basal water pressure, as they are not typically directly connected with the subglacial hydrological system (Downs et al., 2018; Hewitt, 2013).

Models typically treat storage as homogeneous, and therefore independent of vertical position (Banwell et al., 2016; Flowers & Clarke, 2002; Flowers, 2015; De Fleurian et al., 2018). However, storage is a function of depth (Figure 7). We find that the storage volume, or englacial void, that will affect basal water pressure dynamics in the channelized and surrounding distributed portions of the bed is the volume of moulins and connected crevasses within the range of head variation. The equilibrium head h_{eq} in a moulin (Meierbachtol et al., 2013; Röthlisberger, 1972), which is not influenced by the moulin shape but by the glacier characteristics (e.g. ice thickness, subglacial channel length) and the rate of discharge, can be predicted and is shown in Supporting Figure S4 for a wide range of mean meltwater inputs. The size and shape of the storage volume near equilibrium head, which is expected to be up to a few hundreds of meters below the surface, likely controls the amplitude and shape of daily head oscillation and has the ability to filter out meltwater variability with sufficiently high frequency ($f^* \gtrsim 1$). Because moulins are directly connected to the efficient channelized system, the dynamic portion of the moulin may represent a substantial percentage of the englacial void ratio used in subglacial hydrology models.

4.5 The impact of moulin shape on subglacial connectivity and ice speed

While this study investigates how moulin shape modulates water pressures within idealized subglacial channels, we use our results to infer how moulin shape might influence sliding speeds on seasonal timescales. Observed late melt season slowdowns have been attributed to the dewatering of isolated or weakly connected cavities (Andrews et al., 2014; Hoffman et al., 2016) Here, we consider the potential role of moulin shape in this dewatering process by comparing goblet and bottle-shaped moulins to the standard cylindrical shape (Figure 8), which all have the same radius at the equilibrium head h_{eq}.

When compared to a cylindrical moulin (Figure 8a), a goblet-shaped moulin with the same radius at and below the equilibrium head (Figure 8b) will have smaller diurnal water level oscillations, whereas a bottle-shaped moulin (Figure 8c) will have larger oscillations. Larger amplitude water level oscillations should induce stronger subglacial water pressure gradients, forcing water further out into the neighboring distributed drainage system. This could potentially lower pressures within a larger number of weakly connected cavities and connect a larger portion of the surrounding distributed system (Figure 8c). On the other hand, a moulin with smaller oscillations would have less ability to grow connectivity within the surrounding bed.

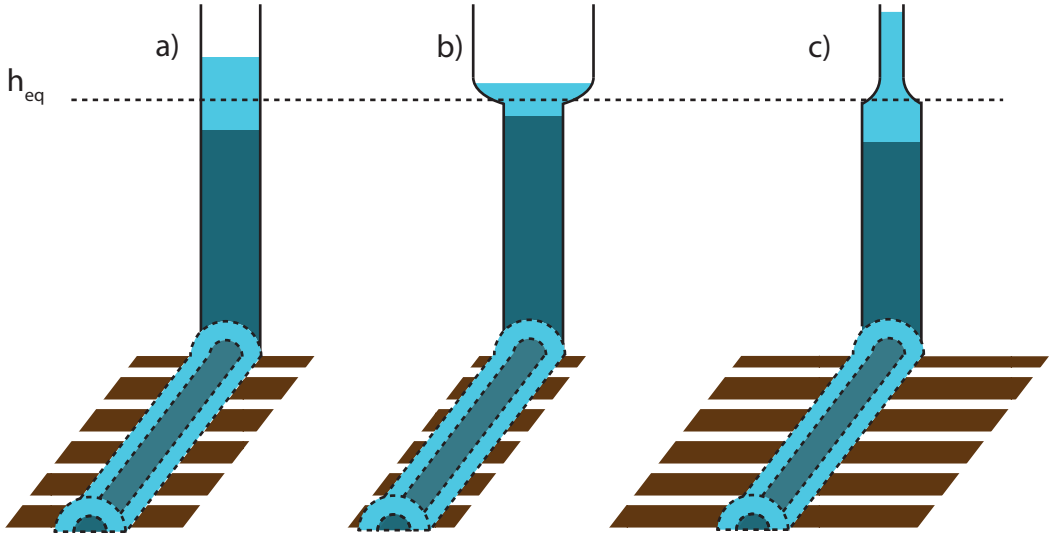

Figure 8. A comparison of the oscillation range for three example moulin shapes and the potential impact on the weakly connected portion of the bed. Light and dark blue indicate the ranges of oscillation in moulin water level and cross-sectional area of the subglacial channel. The brown striations represent the spatial range of influence of the moulin over the surrounding weakly connected bed, with larger pressure oscillations leading to a larger area of influence.

As long-term ice velocities are thought to relate to the weakly connected portion of the bed, short-term pressure variability may play an important part in determining whether early melt season increases in sliding speeds are offset by slowdowns later in the melt season. Our results show that moulin shape and size influence pressure variability. To offer stronger constraints on the impact of moulins over ice-sheet scales, more information is needed on the sizes and shapes of moulins and whether they differ systematically across the ice sheet.

4.6 Complementary approaches to constraining the role of moulins on ice-sheet hydrology

We have shown that equilibration timescales, oscillation amplitude and shape, as well as short-term englacial storage are affected only by volume and changes in volume with height within the head oscillation range. Therefore, characterizing the shapes of the upper portions of moulins will provide constraints for model storage parameters and aid in interpretation of field data.

In order to appropriately represent the englacial storage directly connected to the subglacial channel system, we need to determine not only the moulin density and distribution that can be estimated from satellite imagery (Phillips et al., 2011; Smith et al., 2015), but also the geometry of moulins below the surface. However, if non-cylindrical moulins are prevalent, it may not be possible to infer the cross-sectional areas of moulins relevant for dynamic storage from satellite imagery, or even from surface observations, since volumes at depth may be very different than those observed at the surface. Moulin exploration is difficult, but continued mapping of moulins could provide precious data to constrain the plausible range of dynamic storage volumes within the Greenland Ice Sheet. While exploration and mapping of moulins will provide needed initial information on the typical sizes and shapes of moulins and the factors that influence them, the resources needed in such exploration will limit the number of moulins that can be ex-

plored. Therefore, it is also necessary to understand the processes that lead to the creation of different shapes by modeling of moulin evolution. In this study, we simulated water level within moulins with a static shape. The time evolution and lifetimes of moulins will also likely influence how moulins modulate subglacial water pressures. A physically based model for moulin evolution, informed by field observations from moulin exploration could provide the information needed to extrapolate dynamic storage volumes across an ice sheet scale.

Finally, the model we use represents a single moulin connected to a single channel. In reality, moulins are connected to a network of subglacial channels, exchanging and regulating meltwater inputs with each other. Therefore, understanding how a complex network of moulins interacts will be necessary to get a full picture of the impact of moulins on subglacial pressures. Since prior observations of nearby moulin water levels suggest rapid equilibration of heads through the subglacial system (Andrews et al., 2014), it seems likely that the dynamic storage governing water pressure variability represents an areally-averaged storage volume across many coupled moulins within a region of the ice sheet.

5 Conclusion

We use a simplified model of a subglacial conduit coupled to a moulin to explore relationships between moulin shape and head variation. Our results show that the shape of the moulin within the range of water level oscillations is the main control on the temporal pattern of head dynamics. More specifically, the size of the moulin at and around the equilibrium head position controls the amplitude of the oscillations, while the shape of the moulin controls the shape of the peaks and troughs in water level. We show that the englacial void parameter, used to account for englacial storage in glacial hydrological modeling, can be quantified by moulin volumes at and around h_{eq} (dynamic storage), and not by the overall volume of water held in moulins within a glacier (static storage).

In addition, we find that the dynamic storage of moulins dictates the magnitude of subglacial pressure increases associated with short-term perturbations in supraglacial runoff. The presence of large voids just above the equilibrium head position can strongly dampen the head oscillation amplitudes, even if the rest of the moulin has a relatively small diameter. Such small-amplitude oscillations may inhibit the growth of connectivity within the surrounding weakly connected bed and potentially reduce the mid-to-late-season ice sheet slow down caused by sustained large meltwater inputs to the bed. Future modeling or mapping of moulins would enable better constraints on realistic ranges for dynamic storage within moulins and the controls on that storage, and therefore would improve understanding of the impact of meltwater on ice motion.

Notation

$\boldsymbol{h}$ Moulin hydraulic head
$\boldsymbol{S}$ Subglacial channel cross-sectional area
$\boldsymbol{h_{eq}}$ Moulin equilibrium hydraulic head
$\boldsymbol{dh/dt}$ Rate of change of head over time
$\boldsymbol{r}$ Moulin radius
$\boldsymbol{r_{heq}}$ Moulin radius
$\boldsymbol{r_{top}}$ Moulin radius at the top of the moulin
$\boldsymbol{r_{base}}$ Moulin radius at the base of the moulin
$\boldsymbol{r}$ Moulin radius
$\boldsymbol{A_r}$ Moulin cross-sectional area
$\boldsymbol{A_r(h)}$ Moulin coss-sectional area at the water level
$\boldsymbol{Q_{in}}$ Supraglacial meltwater input
$\boldsymbol{Q_{out}}$ Subglacial channel water output
$\boldsymbol{Q_a}$ Amplitude of oscillation of the meltwater input
$\boldsymbol{Q_{mean}}$ Mean meltwater input
$\boldsymbol{H}$ Ice thickness
$\boldsymbol{H/2}$ Half of the ice thickness
$\boldsymbol{L}$ Subglacial channel length
$\boldsymbol{z}$ Elevation from bedrock
$\boldsymbol{m}$ Moulin wall slope $\Delta r/\Delta z$
$\boldsymbol{\tau_{osc}}$ Period of oscillation timescale
$\boldsymbol{\tau_{damp}}$ Damping E-folding timescale
$\boldsymbol{f^*}$ Non-dimensional meltwater input frequency
$\boldsymbol{a}$ Amplitude of the moulin head oscillation above h_{eq}
$\boldsymbol{\kappa}$ Peakedness of the moulin head oscillation in the vicinity of the peak

6 Open Research

The code (in Python) used to make the simulations and create the figures is available in the public Github repository `https://github.com/cctrunz/ModelRepo_MoulinShapeStoragePaper.git`. The current version of the model repository is the release v.2 (Trunz, 2022) and is archived by Zenodo `https://zenodo.org/record/6338955`.

Acknowledgments

C.T., M.D.C., J.M., and J.G. were supported by the United States National Science Foundation grants 1604022. K.P. and L.C.A. received support from NASA Cryosphere award 80NSSC19K0054. The authors declare there are no conflicts of interest with regard to finances or with the results of this paper.

References

Andrews, L. C., Catania, G. A., Hoffman, M., Gulley, J., Lüthi, M. P., Ryser, C., ... Neumann, T. A. (2014). Direct observations of evolving subglacial drainage beneath the Greenland Ice Sheet. *Nature*, *514*(7520), 80–83. doi: 10.1038/nature13796

Andrews, L. C., Poinar, K., & Trunz, C. (2021). Controls on Greenland moulin geometry and evolution from the Moulin Shape model. *The Cryosphere Discussions*, 1–47. doi: doi.org/10.5194/tc-2021-41

Arnold, N., Richards, K., Willis, I., & Sharp, M. (1998). Initial results from a distributed, physically based model of glacier hydrology. *Hydrological Processes*,

12(2), 191–219.

Banwell, A., Hewitt, I., Willis, I., & Arnold, N. (2016). Moulin density controls drainage development beneath the Greenland ice sheet. *Journal of Geophysical Research: Earth Surface*, *121*(12), 2248–2269. doi: 10.1002/2015JF003801

Bartholomaus, T. C., Anderson, R. S., & Anderson, S. P. (2011). Growth and collapse of the distributed subglacial hydrologic system of Kennicott Glacier, Alaska, USA, and its effects on basal motion. *Journal of Glaciology*, *57*(206), 985–1002. doi: 10.3189/002214311798843269

Bartholomew, I., Nienow, P., Sole, A., Mair, D., Cowton, T., & King, M. A. (2012). Short-term variability in Greenland Ice Sheet motion forced by time-varying meltwater drainage: Implications for the relationship between subglacial drainage system behavior and ice velocity. *Journal of Geophysical Research: Earth Surface*, *117*(3), F03002. doi: 10.1029/2011JF002220

Bourseiller, P., Lamberton, J., Moreau, L., Couté, A., & Quennehen, C. (2002). *Voyage dans les glaces*. Paris: La Martinière Jeunesse.

Catania, G. A., & Neumann, T. A. (2010). Persistent englacial drainage features in the Greenland Ice Sheet. *Geophysical Research Letters*, *37*(2), L02501. doi: 10.1029/2009GL041108

Catania, G. A., Neumann, T. A., & Price, S. F. (2008). Characterizing englacial drainage in the ablation zone of the Greenland ice sheet. *Journal of Glaciology*, *54*(187), 567–578. doi: 10.3189/002214308786570854

Clarke, G. K. C. (1996). Lumped-element analysis of subglacial hydraulic circuits. *Journal of Geophysical Research: Solid Earth*, *101*(B8), 17547–17559. doi: 10.1029/96JB01508

Colgan, W., Steffen, K., McLamb, W. S., Abdalati, W., Rajaram, H., Motyka, R., ... Anderson, R. (2011). An increase in crevasse extent, West Greenland: Hydrologic implications. *Geophysical Research Letters*, *38*(18), L18502. doi: 10.1029/2011GL048491

Covington, M. D., Banwell, A., Gulley, J., Saar, M. O., Willis, I., & Wicks, C. M. (2012). Quantifying the effects of glacier conduit geometry and recharge on proglacial hydrograph form. *Journal of Hydrology*, *414*, 59–71. doi: 10.1016/j.jhydrol.2011.10.027

Covington, M. D., Gulley, J. D., Trunz, C., Mejia, J., & Gadd, W. (2020). Moulin Volumes Regulate Subglacial Water Pressure on the Greenland Ice Sheet. *Geophysical Research Letters*, *47*(20). doi: 10.1029/2020GL088901

Covington, M. D., Wicks, C. M., & Saar, M. O. (2009). A dimensionless number describing the effects of recharge and geometry on discharge from simple karstic aquifers. *Water Resources Research*, *45*(11), W11410. doi: 10.1029/2009WR008004

Cowton, T., Nienow, P., Sole, A., Bartholomew, I., & Mair, D. (2016). Variability in ice motion at a land-terminating Greenlandic outlet glacier: the role of channelized and distributed drainage systems. *Journal of Glaciology*, *62*(233), 451–466. doi: 10.1017/jog.2016.36

De Fleurian, B., Werder, M. A., Beyer, S., Brinkerhoff, D. J., Delaney, I., Dow, C. F., ... Sommers, A. N. (2018). SHMIP The subglacial hydrology model intercomparison Project. *Journal of Glaciology*, *64*(248), 897–916. doi: 10.1017/jog.2018.78

Dow, C. F., Kulessa, B., Rutt, I. C., Doyle, S. H., & Hubbard, A. (2014). Upper bounds on subglacial channel development for interior regions of the Greenland ice sheet. *Journal of Glaciology*, *60*(224), 1044–1052. doi: 10.3189/2014JoG14J093

Downs, J. Z., Johnson, J. V., Harper, J. T., Meierbachtol, T., & Werder, M. A. (2018). Dynamic Hydraulic Conductivity Reconciles Mismatch Between Modeled and Observed Winter Subglacial Water Pressure. *Journal of Geophysical Research: Earth Surface*, *123*(4), 818–836. doi: 10.1002/2017JF004522

Flowers, G. E. (2015). Modelling water flow under glaciers and ice sheets. *Proc. R. Soc. A*, *471*(2176), 20140907. doi: 10.1098/rspa.2014.0907

Flowers, G. E., & Clarke, G. K. C. (2002). A multicomponent coupled model of glacier hydrology 1. Theory and synthetic examples. *Journal of Geophysical Research: Solid Earth*, *107*(B11), 2287. doi: 10.1029/2001JB001122

Griselin, M. (1995). *3e symposium international, cavités glaciaires et cryokarst en régions polaires et de haute montagne: Chamonix-France, 1er-6 novembre 1994 : actes.* Presses Univ. Franche-Comté.

Gulley, J., Benn, D., Screaton, E., & Martin, J. (2009). Mechanisms of englacial conduit formation and their implications for subglacial recharge. *Quaternary Science Reviews*, *28*(19-20), 1984–1999. doi: 10.1016/j.quascirev.2009.04.002

Gulley, J., Walthard, P., Martin, J., Banwell, A., Benn, D., & Catania, G. (2012). Conduit roughness and dye-trace breakthrough curves: why slow velocity and high dispersivity may not reflect flow in distributed systems. *Journal of Glaciology*, *58*(211), 915–925. doi: 10.3189/2012JoG11J115

Harper, J. T., Bradford, J. H., Humphrey, N. F., & Meierbachtol, T. W. (2010). Vertical extension of the subglacial drainage system into basal crevasses. *Nature; London*, *467*(7315), 579–82. doi: 10.1038/nature09398

Hewitt, I. (2013). Seasonal changes in ice sheet motion due to melt water lubrication. *Earth and Planetary Science Letters*, *371-372*, 16–25. doi: 10.1016/j.epsl.2013.04.022

Hewitt, I., Schoof, C., & Werder, M. A. (2012). Flotation and free surface flow in a model for subglacial drainage. Part 2. Channel flow. *Journal of Fluid Mechanics*, *702*, 157–187. doi: 10.1017/jfm.2012.166

Hoffman, M., Andrews, L. C., Price, S. A., Catania, G. A., Neumann, T. A., Luthi, M. P., ... Morriss, B. (2016). Greenland subglacial drainage evolution regulated by weakly connected regions of the bed. *Nature Communications*, *7*(13903). doi: 10.1038/ncomms13903

Holmlund, P. (1988). Internal Geometry and Evolution of Moulins, Storglaciären, Sweden. *Journal of Glaciology*, *34*(117), 242–248. doi: 10.1017/S0022143000032305

King, L. A. (2018). *Identifying and characterizing the spatial variability of supraglacial hydrological features on the western Greenland Ice Sheet* (Doctoral dissertation, University of British Columbia). doi: 10.14288/1.0372827

Koziol, C. P., & Arnold, N. (2018). Modelling seasonal meltwater forcing of the velocity of land-terminating margins of the Greenland Ice Sheet. *Cryosphere*, *12*(3), 971–991. doi: 10.5194/tc-12-971-2018

Lamberton, J. (2002). *Les moulins de glace: mémoires d'un glacionaute.* Paris: Hoëbeke.

McGrath, D., Colgan, W., Steffen, K., Lauffenburger, P., & Balog, J. (2011). Assessing the summer water budget of a moulin basin in the Sermeq Avannarleq ablation region, Greenland ice sheet. *Journal of Glaciology*, *57*(205), 954–964. doi: 10.3189/002214311798043735

Meierbachtol, T., Harper, J., & Humphrey, N. (2013). Basal Drainage System Response to Increasing Surface Melt on the Greenland Ice Sheet. *Science*, *341*(6147), 777–779. doi: 10.1126/science.1235905

Mejia, J. Z., Gulley, J. D., Trunz, C., Covington, M. D., Bartholomaus, T. C., Xie, S., & Dixon, T. H. (2021). Isolated Cavities Dominate Greenland Ice Sheet Dynamic Response to Lake Drainage. *Geophysical Research Letters*, *48*(19), e2021GL094762. doi: 10.1029/2021GL094762

Moreau, L. (2009). L'exploration du cryokarst glaciaire et son intérêt scientifique pour l'étude du drainage des eaux de fonte : porches, cavités, crevasses, bédières et moulins. *Collection EDYTEM. Cahiers de géographie*, *8*(1), 163–170. doi: 10.3406/edyte.2009.1083

Nye, J. F. (1976). Water Flow in Glaciers: Jökulhlaups, Tunnels and Veins. *Journal*

of Glaciology, *17*(76), 181–207. doi: 10.3189/S002214300001354X

Phillips, T., Leyk, S., Rajaram, H., Colgan, W., Abdalati, W., McGrath, D., & Steffen, K. (2011). Modeling moulin distribution on Sermeq Avannarleq glacier using ASTER and WorldView imagery and fuzzy set theory. *Remote Sensing of Environment*, *115*(9), 2292–2301. doi: 10.1016/j.rse.2011.04.029

Poinar, K., Joughin, I., Lilien, D., Brucker, L., Kehrl, L., & Nowicki, S. (2017). Drainage of Southeast Greenland Firn Aquifer Water through Crevasses to the Bed. *Frontiers in Earth Science*, *5*. doi: 10.3389/feart.2017.00005

Reynaud, L., & Moreau, L. (1994). Moulins glaciaires des glaciers tempérés et froids de 1986 à 1994 (Mer de Glace et Groenland) : morphologie et techniques de mesures de la déformation de la glace. Paris.

Röthlisberger, H. (1972). Water Pressure in Intra- and Subglacial Channels. *Journal of Glaciology*, *11*(62), 177–203. doi: 10.1017/S0022143000022188

Schoof, C. (2010). Ice-sheet acceleration driven by melt supply variability. *Nature*, *468*(7325), 803–806. doi: 10.1038/nature09618

Smith, L. C., Chu, V. W., Yang, K., Gleason, C. J., Pitcher, L. H., Rennermalm, A. K., ... Balog, J. (2015). Efficient meltwater drainage through supraglacial streams and rivers on the southwest Greenland ice sheet. *PNAS*, *112*(4), 1001–1006. doi: 10.1073/pnas.1413024112

Sommers, A., Rajaram, H., & Morlighem, M. (2018). SHAKTI Subglacial Hydrology and Kinetic, Transient Interactions v1.0. *Geoscientific Model Development*, *11*(7), 2955–2974. doi: 10.5194/gmd-11-2955-2018

Spring, U., & Hutter, K. (1981). Numerical studies of jökulhlaups. *Cold Regions Science and Technology*, *4*(3), 227–244.

Stevens, L. A., Hewitt, I. J., Das, S. B., & Behn, M. D. (2018). Relationship Between Greenland Ice Sheet Surface Speed and Modeled Effective Pressure. *Journal of Geophysical Research: Earth Surface*, *123*(9), 2258–2278. doi: 10.1029/2017JF004581

Stubblefield, A. G., Creyts, T. T., Kingslake, J., & Spiegelman, M. (2019). Modeling oscillations in connected glacial lakes. *Journal of Glaciology*, *65*(253), 745 – 758. doi: 10.1017/jog.2019.46

Trunz, C. (2021). *Modeling and Measuring Water Level Fluctuations in the Greenland Ice Sheet: How Moulin Life Cycle and Shape can Inform us on the Subglacial Drainage System.* (Doctoral Thesis). University of Arkansas, Fayetteville.

Trunz, C. (2022, March). *cctrunz/ModelRepo_moulinshapestoragepaper: Release v.2.* Zenodo. Retrieved 2022-03-08, from `https://zenodo.org/record/6338955` doi: \ci

Vallot, J. (1898). Exploration des moulins de la Mer de Glace. *Annales de l'Observatoire météorologique du Mont-Blanc*, *3*(1), 183–193.

van der Veen, C. J. (1998). Fracture mechanics approach to penetration of bottom crevasses on glaciers. *Cold Regions Science and Technology*, *27*(3), 213–223. doi: 10.1016/S0165-232X(98)00006-8

Vatne, G., & Irvine-Fynn, T. D. L. (2016). Morphological dynamics of an englacial channel. *Hydrology and Earth System Sciences*, *20*(7), 2947–2964. doi: 10.5194/hess-20-2947-2016

Werder, M. A., Hewitt, I. J., Schoof, C., & Flowers, G. E. (2013). Modeling channelized and distributed subglacial drainage in two dimensions. *Journal of Geophysical Research: Earth Surface*, *118*(4), 2140–2158. doi: 10.1002/jgrf.20146

Werder, M. A., Schuler, T. V., & Funk, M. (2010). Short term variations of tracer transit speed on alpine glaciers. *The Cryosphere*, *4*(3), 381–396. doi: 10.5194/tc-4-381-2010

Wright, P. J., Harper, J. T., Humphrey, N. F., & Meierbachtol, T. W. (2016). Measured basal water pressure variability of the western Greenland Ice Sheet: Implications for hydraulic potential: Greenland Ice Sheet Basal Water Pres-

sure. *Journal of Geophysical Research: Earth Surface*, *121*(6), 1134–1147. doi: 10.1002/2016JF003819

Supporting Information for "Modeling the impact of moulin shape on englacial hydrology"

Celia TRUNZ[1], Matthew D. COVINGTON[1], Kristin POINAR[2],

Lauren C. ANDREWS[3], Jessica MEJIA[2,4], Jason GULLEY[4]

[1]Geosciences Department, University of Arkansas, Fayetteville AR, USA

[2]Department of Geology, University at Buffalo, Buffalo NY, USA

[3]Global Modeling and Assimilation Office, NASA Goddard Space Flight Center, Greenbelt MD, USA

[4]Geosciences Department, University of South Florida, Tampa FL, USA

Contents of this file

1. Text S1 to S3

2. Figures S1 to S6

3. Tables S1 to S6

Introduction The supporting information provides additional information about the simulations and methods. **Text S1** shows the derivation for the change in head with cylindrical and non-cylindrical moulins. **Text S2** describes our moulin shape parameterization for constant meltwater input. **Text S3** describe the 1D discretized version of the single-conduit model used to compare the 0D version of the model used throughout the paper. **Figure S1** and **Figure S2** provide visualizations of the damping and oscillation

Corresponding author: celia.trunz@gmail.com

timescales. **Figure S3** is an additional figure showing how an abrupt change in radius impacts the equilibration timescales. **Figure S4** demonstrates how the equilibrium head changes across the ice sheet. **Figure S5** shows the parametrization of moulin shape for an oscillating meltwater input. **Figure S6** compares the single-conduit model with a discretized subglacial channel model. **Table S1 to S6** summarize the input and fitting parameters for all the simulations and figures in the paper.

Text S1. Here we derive the moulin radius as a function of elevation

Case for a cylinder:

The continuity equation says that for Δt, the change in storage, ΔV, equals the input meltwater, Q_{in}, minus the discharge out of the channel, Q_{out}, times Δt, or

$$\frac{\Delta V}{\Delta t} = Q_{in} - Q_{out} \tag{1}$$

For each time-step, the **storage of water** $\Delta V = A_{\mathrm{r}} \Delta h$. If we plug in this relationship to Equation 1, then we get:

$$\frac{\Delta (h A_{\mathrm{r}})}{\Delta t} = Q_{in} - Q_{out} \tag{2}$$

If we rearrange then we obtain:

$$\frac{\Delta h}{\Delta t} = \frac{Q_{in} - Q_{out}}{A_{\mathrm{r}}} \tag{3}$$

If $\Delta t \longrightarrow 0$ then:

$$\lim_{\Delta t \to 0} [\frac{\Delta h}{\Delta t}] = \frac{dh}{dt} \Rightarrow \frac{dh}{dt} = \frac{Q_{in} - Q_{out}}{A_{\mathrm{r}}} \tag{4}$$

Case for a conical frustum:

If we use Equation 1 and plug in the volume of a frustum $\Delta V = \frac{1}{3}\pi(r_{\text{top}}^2 + r_{\text{top}}r_{\text{base}} + r_{\text{base}}^2) * \Delta h$. We obtain

$$\frac{\Delta h}{\Delta t} = \frac{Q_{in} - Q_{out}}{\frac{1}{3}\pi(r_{\text{top}}^2 + r_{\text{top}}r_{\text{base}} + r_{\text{base}}^2)} \tag{5}$$

We then define $r_{\text{top}}, r_{\text{base}}$ w.r.t. Δh or Δt. The slope $m = \frac{\Delta h}{\Delta r}$ and the change between the radius $\Delta r = r_{\text{base}} - r_{\text{top}} = \frac{\Delta h}{m}$. Therefore, we can express $r_{\text{base}} = r_{\text{top}} + \frac{\Delta h}{m}$ and replace r_{base} in Equation 5, giving

$$\frac{\Delta h}{\Delta t} = \frac{Q_{in} - Q_{out}}{\frac{\pi}{3}r_{\text{top}}^2 + [r_{\text{top}}(r_{\text{top}} + \frac{\Delta h}{m})] + (r_{\text{top}} + \frac{\Delta h}{m})^2} \tag{6}$$

We distribute and reorganize the denominator and get

$$\frac{\Delta h}{\Delta t} = \frac{Q_{in} - Q_{out}}{\pi r_{\text{top}}^2 + \pi r_{\text{top}}\frac{\Delta h}{m} + \frac{\pi}{3}\frac{\Delta h^2}{m^2}} \tag{7}$$

If $\Delta t \longrightarrow 0$, $\Delta h \longrightarrow 0$, then $\frac{2r_{\text{top}}\Delta h}{m}$ and $\frac{\Delta h^2}{m^2} \longrightarrow 0$, we are left with πr^2 at the denominator and we recover the continuity equation (1) for a cylindrical moulin:

$$\frac{dh}{dt} = \frac{Q_{in} - Q_{out}}{\pi r^2} = \frac{Q_{in} - Q_{out}}{A_{\text{r}}} \tag{8}$$

Text S2. Here we describe our moulin shape parameterization for constant meltwater input. We use a cone-shaped moulin with various wall slopes and the radius fixed at a certain depth. To explore equilibration timescales, we use a conical frustum where r_{base}/r_{top} can be greater than or less than 0.

$$A_{\text{r}}(z) = \pi(mz + r_{base})^2 \tag{9}$$

To fix the radius at the middle of the ice thickness, we define the base radius to be

$$r_{base} = r_{h_{\text{eq}}} - m(H/2) \tag{10}$$

. To fix the radius at equilibrium head, we define the base radius to be

$$r_{base} = r_{h_{\text{eq}}} - mh_{\text{eq}} \tag{11}$$

Text S3.

Here we describe the discretized subglacial channel model used as a comparison in Supplemental Figure S6. The model uses Equations 1-3 from the main text, which are the same as for the 0D model described in the model description Section 2 in the main text. However, instead of calculating the effective pressure at the moulin only, we use a one dimensional grid set up from Landlab (Hobley et al., 2017) with nodes every 400m along the conduits. At each node calculate the hydraulic gradient as well as the conduit cross-section evolution via melt and creep for every node along the conduit. The ice thickness is calculated with the square-root glacier function from equation 5 in Section 2. The code for the 1D model is in `https://github.com/speleophysics/landlab/tree/add-pressurized-flow-network-solver/landlab/components/conduit_networks`.

References

Hobley, D. E. J., Adams, J. M., Nudurupati, S. S., Hutton, E. W. H., Gasparini, N. M., Istanbulluoglu, E., & Tucker, G. E. (2017). Creative computing with Landlab: an open-source toolkit for building, coupling, and exploring two-dimensional numerical models of Earth-surface dynamics. *Earth Surface Dynamics*, *5*(1), 21–46. doi: 10.5194/esurf-5-21-2017

Meierbachtol, T., Harper, J., & Humphrey, N. (2013). Basal Drainage System Response to Increasing Surface Melt on the Greenland Ice Sheet. *Science*, *341*(6147), 777–779. doi: 10.1126/science.1235905

Röthlisberger, H. (1972). Water Pressure in Intra- and Subglacial Channels. *Journal of Glaciology*, *11*(62), 177–203. doi: 10.1017/S0022143000022188

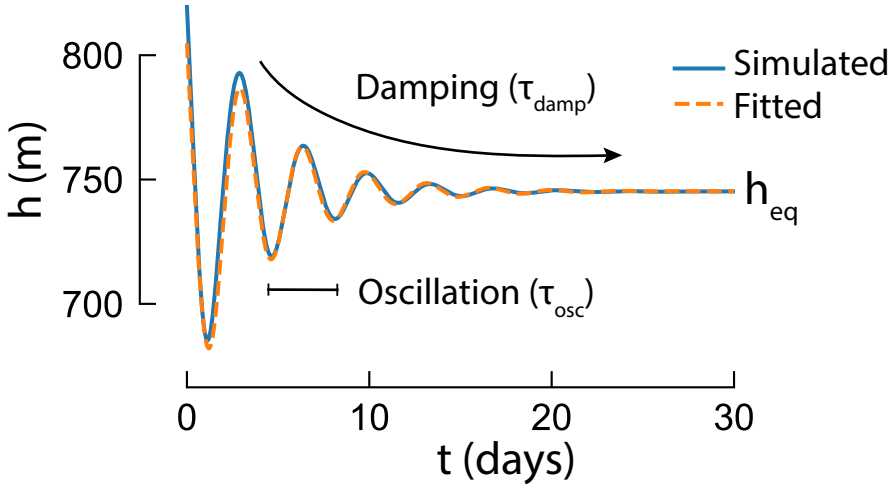

Figure S1. Oscillation of head during equilibration. The solid line shows the full numerical result, and the dashed line shows the fit of an idealized solution for a damped harmonic oscillator. The simulation is for a cylindrical moulin, with $Q_{\text{in}} = 3\,\text{m}^3/\text{s}$ and $r = 10\,\text{m}$.

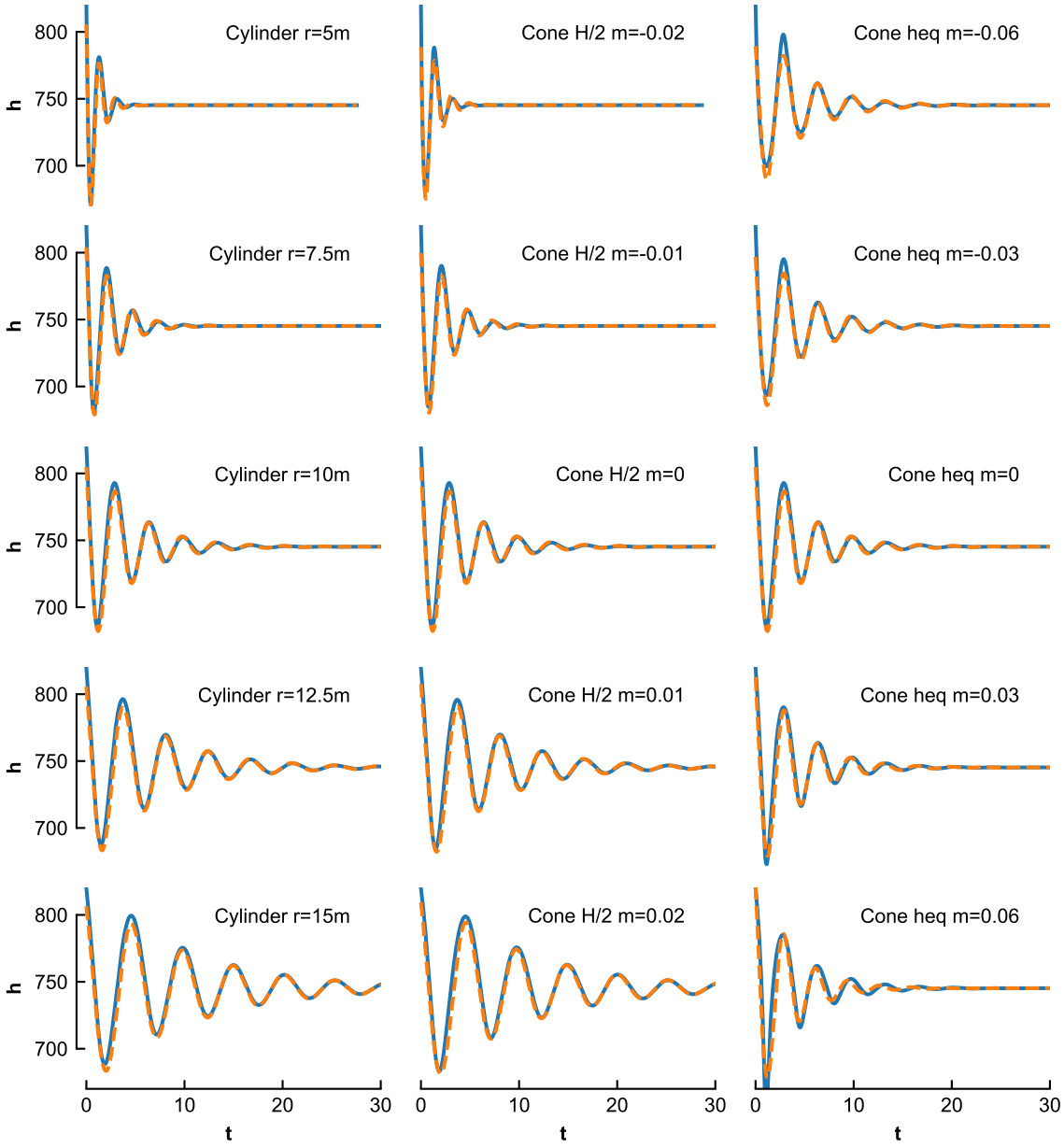

Figure S2. Comparison between simulated and fitted oscillations for many cases.

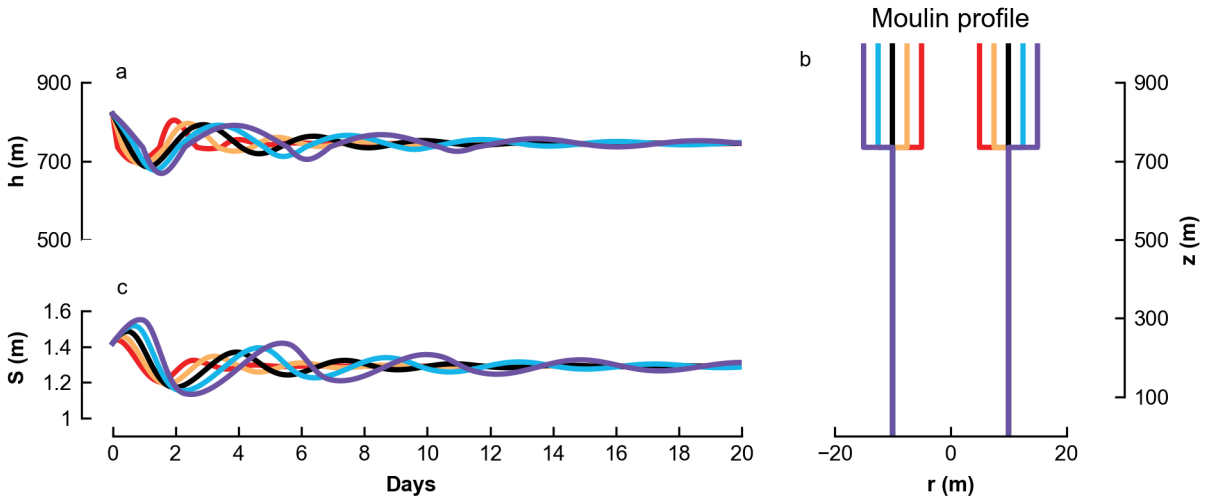

Figure S3. Timeseries of **head (h)** and **channel cross-sectional area (S)** for a fixed meltwater input Q_{in} for bottle-shaped moulins (red and yellow), a cylindrical moulin (black) and goblet-shaped moulins (blue and purple)

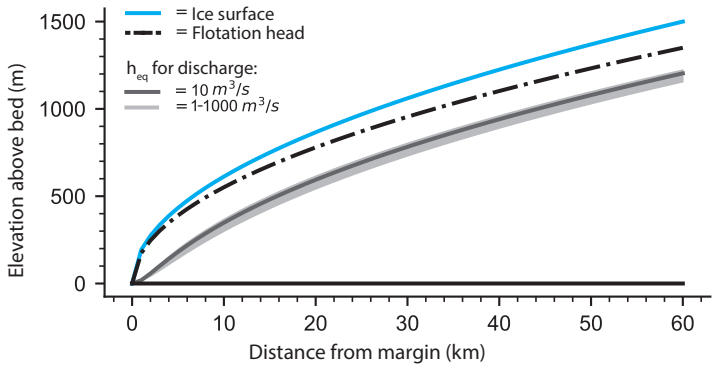

Figure S4. Equilibrium head (h_{eq}) along an ice sheet profile for a wide range of Q_{in}. Equilibrium head (h_{eq}) calculated with the model depends on channel length, ice thickness, and Q_{in}. Meierbachtol et al. (2013); Röthlisberger (1972) described similar profiles.

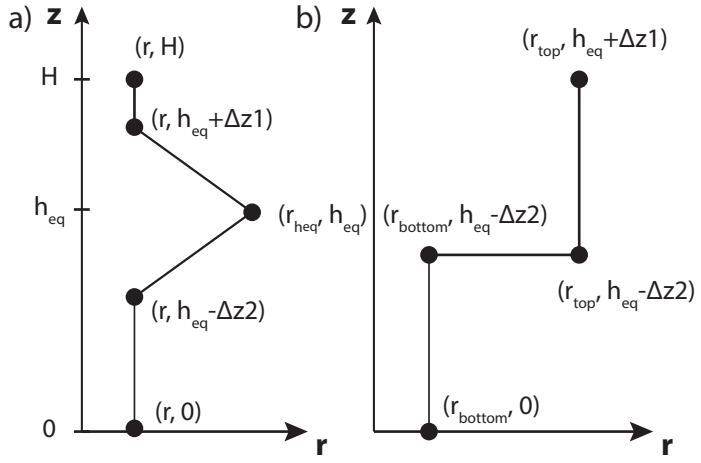

Figure S5. Cartesian coordinates of the moulin shape used for the simulation with oscillating meltwater input. Parameterization for hourglass, diamond and superposed-cylinder shaped moulin. To explore oscillating meltwater input, we define the shape by interpolating the radius defined in the cartesian coordinate system, with r in the x axis, and z in the y axis. Shape coordinates are displayed in Figure S6. The radius (r) is interpolated every meter along the axis z. (a) Hourglass and diamond shaped moulins are defined by five points. (b) Goblet and bottle-shaped moulins defined by four points.

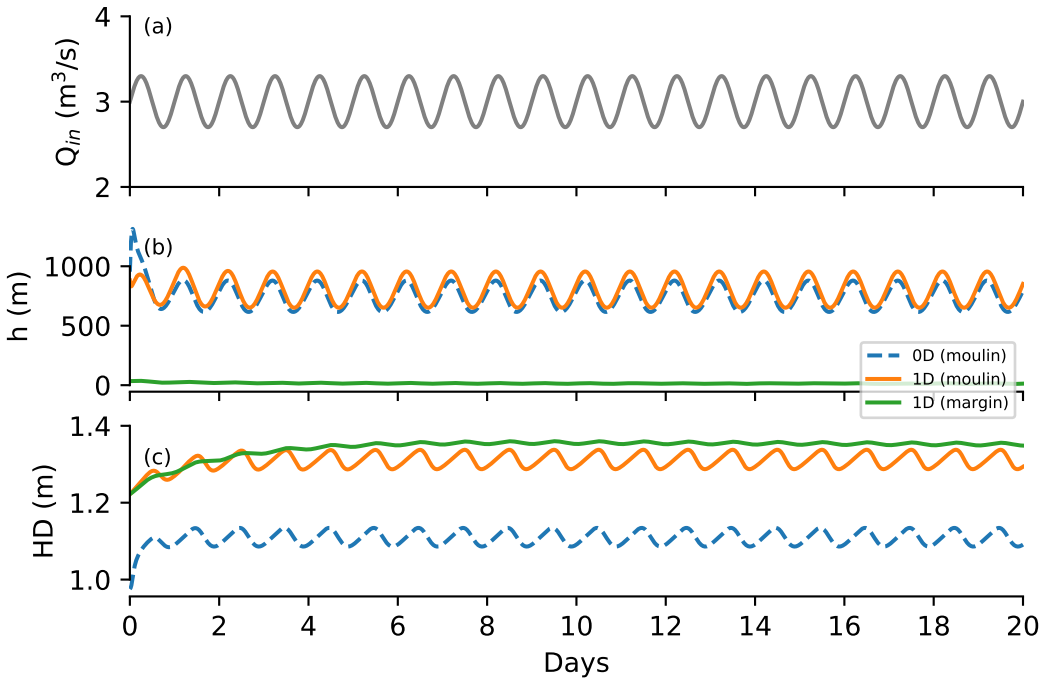

Figure S6. Comparison between the 0D single-conduit model used in the paper and a similar 1D single-conduit model, where each node along the conduit has a different effective pressure and cross-sectional area, using an idealized square-root glacier (see equation 5 in Section 2). (a) Meltwater input (Q_{in}): we use the same sinusoidal meltwater input as for the simulations in the paper: $Q_{\text{mean}} = 3\,\text{m}^3/\text{s}$, $Q_{\text{min}} = 2.6\,\text{m}^3/\text{s}$; (b) Hydraulic head and (c) Hydraulic diameter (HD) at the moulin for the 0D and the 1D model, and at the margin for the 1D model.

Table S1. Constants and model parameters used in the simulations.

Symbol	Value	Description
ρ_{w}	1000 kg/m^3	Water density
ρ_{i}	910 kg/m^3	Ice density
g	9.8 m/s^2	Gravitational acceleration
f	0.1	Darcy-Weissbach friction factor
L_f	3.32e5 J/kg	Latent heat of fusion
B	6e-24 $1/Pa^3s$	Glen's law fluidity coefficient (Basal softness)
n	3	Glen's law exponent
C_1	$1/(\rho_{\mathrm{i}} * L_f)$	Melt opening parameter
C_2	$2Bn^{-n}$	Closure parameter
C_3	$2^{5/4}\sqrt{\pi}/(\pi^{1/4}\sqrt{\pi+2}\sqrt{\rho_{\mathrm{w}}f})$	Flux parameter

Table S2. Model parameters for simulations with constant Q_{in} in Figure 2 (main text). For the simulations with this parameters, the equilibrium head $h_{\mathrm{eq}} = 745$, and equilibrium subglacial channel cross-section area $S_{\mathrm{eq}} = 1.3$

Parameter	Value	Unit	Description
Q_{in}	3	m^3/s	Constant meltwater input
t_0	0	d	Initial time
t_{f}	100	d	Final time
H_0	6	m	Ice thickness
h_0	$1.1h_{\mathrm{eq}}$	m	Initial head
S_0	$1.1S_{\mathrm{eq}}$	m	Initial subglacial channel cross-section

Table S3. Moulin shape parameters for simulations with constant Q_{in} in Figure 2 (main text). The radius (r) is in meters and the slope (m) is given in percent (%) and degrees (°) from the vertical axis.

plot color	red	yellow	black	blue	purple
Cylinder					
m	0	0	0	0	0
r	5	7.5	10	12.5	15
Cone $H/2$					
$m\%$	-2	-1	0	1	2
m°	-1.15	-0.57	0	0.57	1.15
r_{middle}	10	10	10	10	10
r_{heq}	5	7.5	10	12.5	15
r_{base}	20	15	10	5	0
r_{top}	0	5	10	15	20
Cone h_{eq}					
$m\%$	-6	-3	0	3	6
m°	-3.43	-1.72	0	1.72	3.43
r_{heq}	10	10	10	10	10
r_{base}	25	17.5	10	2.5	-5
r_{top}	5	7.5	10	12.5	15
Diamond-Hourglass h_{eq}					
$m\%$	-6	-3	0	3	6
m°	-3.43	-1.72	0	1.72	3.43
r_{heq}	10	10	10	10	10

Table S4. Fitting parameters for simulations in Figure 2 (main text). The damping timescale (τ_{damp}), the period of oscillation (τ_{osc}), the amplitude (a) in meters, and the phase shift (ϕ) in days. A visual comparison between simulations and fits is provided in Figure S2.

Cylinder	radius	τ_{damp}	τ_{osc}	a	ϕ
red	5.0	0.94	1.64	0.14	2.65
yellow	7.5	2.23	2.53	0.11	2.49
black	10.0	4.08	3.42	0.09	2.37
blue	12.5	6.61	4.30	0.09	2.28
purple	15.0	10.00	5.18	0.08	2.20

Cone $H/2$	slope	τ_{damp}	τ_{osc}	a	ϕ
red	-0.02	1.18	1.75	0.12	2.73
yellow	-0.01	2.34	2.56	0.10	2.52
black	0.00	4.08	3.42	0.09	2.37
blue	0.01	6.53	4.28	0.09	2.26
purple	0.02	9.87	5.14	0.09	2.18

Cone h_{eq}	slope	τ_{damp}	τ_{osc}	a	ϕ
red	-0.06	4.22	3.44	0.08	2.49
yellow	-0.03	4.18	3.43	0.09	2.43
black	0.00	4.08	3.42	0.09	2.37
blue	0.03	3.86	3.37	0.10	2.31
purple	0.06	3.29	3.25	0.11	2.24

Diamond-Hourglass h_{eq}	slope	τ_{damp}	τ_{osc}	a	ϕ
red	-0.06	2.71	3.03	0.09	2.59
yellow	-0.03	3.40	3.23	0.09	2.48
black	0.00	4.08	3.42	0.09	2.37
blue	0.03	4.75	3.61	0.10	2.25
purple	0.06	5.39	3.81	0.10	2.14

Table S5. Model parameters from graphs for oscillating Q_{in}, Figure 4 and 5 (main text).

Parameter	Value	Unit	Description
Q_{mean}	3	m^3/s	Mean meltwater input
Q_{a}	0.4	m^3/s	Amplitude of oscillation of the meltwater input
Q_{period}	1	d	Period of oscillation of meltwater input
t_0	0	d	Initial time
t_{f}	50	d	Final time
H	1000	m	Ice thickness
L	30000	m	Subglacial channel length

Table S6. Moulin shape parameters from graphs for oscillating Q_{in}, Figure 4 and 5 (main text). The radius (r) is in meters.

cylinder	red	yellow	black	blue	purple
r (m)	1	3.5	5	8	15

Hourglass-Diamond 1	red	yellow	black	blue	purple
r	1	2	5	10	19
r_{heq}	5	5	5	5	5

Hourglass-Diamond 2	red	yellow	black	blue	purple
r	5	5	5	5	5
r_{heq}	1	3.5	5	8	15

Diamond	red	yellow	black	blue	purple
r	1	1.5	2	4	10
r_{heq}	5	5.5	6	8	14

Hourglass	red	yellow	black	blue	purple
r	5	6.5	8	10	18
r_{heq}	1	2.5	4	6	14

Bottle-Goblet 1	red	yellow	black	blue	purple
r_{top}	3	4	5	6	10
r_{base}	5	5	5	5	5

Bottle-Goblet 2	red	yellow	black	blue	purple
r_{top}	5	5	5	5	5
r_{base}	1	2	4	6	12